iScience

CellPress
OPEN ACCESS

Article

Structural basis for selective inhibition of human serine hydroxymethyltransferase by secondary bile acid conjugate

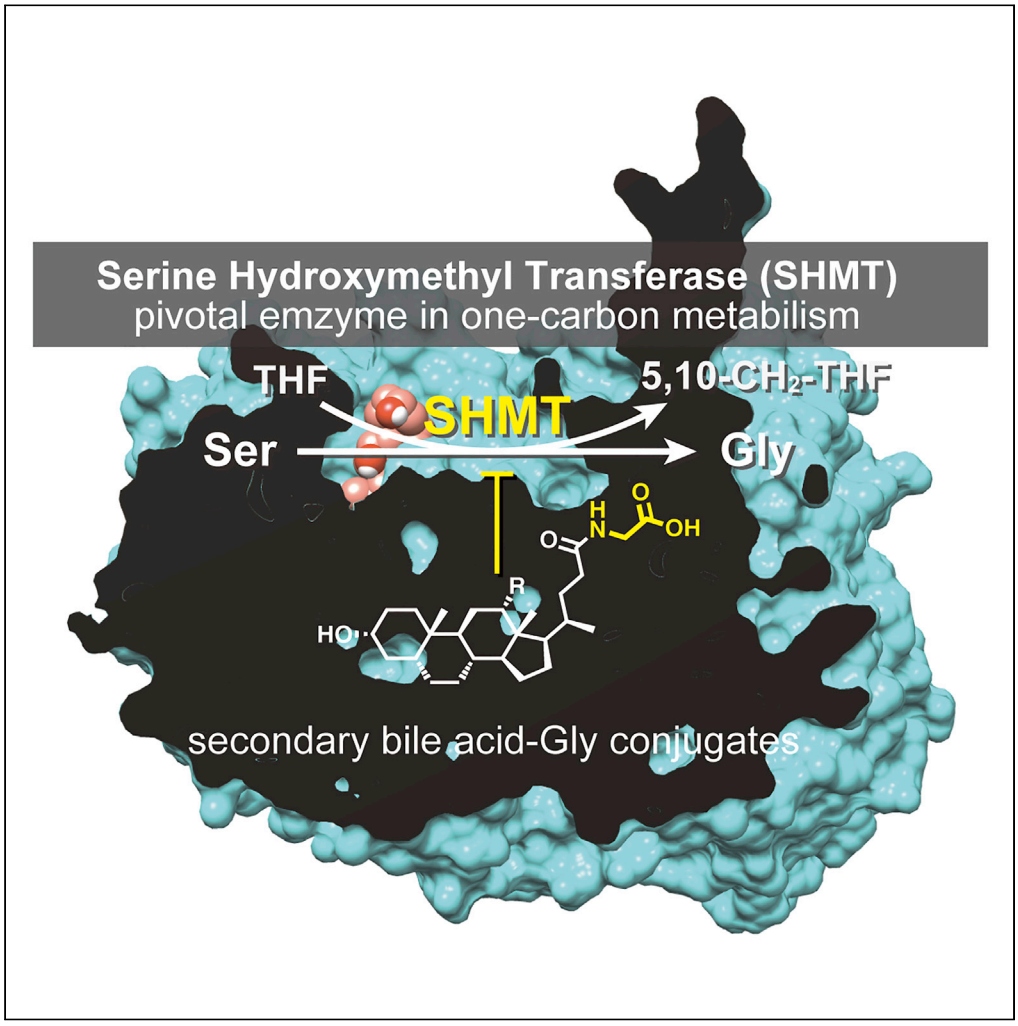

Tomoki Ota, Akinobu Senoo, Masumi Shirakawa, ..., Satoru Nagatoishi, Kouhei Tsumoto, Shinsuke Sando

ssando@chembio.t.u-tokyo.ac.jp

HIGHLIGHTS

The crystal structures of hSHMT in complex with secondary bile acid glycine conjugate

Specific interactions between hSHMT and secondary bile acid conjugate were validated

Biological role of bile acids as modulators for one-carbon metabolism is suggested

Ota et al., iScience *24*, 102036
February 19, 2021
https://doi.org/10.1016/j.isci.2021.102036

iScience

CellPress
OPEN ACCESS

Article

Structural basis for selective inhibition of human serine hydroxymethyltransferase by secondary bile acid conjugate

Tomoki Ota,[1,7] Akinobu Senoo,[1,7] Masumi Shirakawa,[1,7] Hiroshi Nonaka,[1] Yutaro Saito,[1] Sho Ito,[2,3] Go Ueno,[4] Satoru Nagatoishi,[5] Kouhei Tsumoto,[1,5,6] and Shinsuke Sando[1,6,8,*]

SUMMARY

Bile acids are metabolites of cholesterol that facilitate lipid digestion and absorption in the small bowel. Bile acids work as agonists of receptors to regulate their own metabolism. Bile acids also regulate other biological systems such as sugar metabolism, intestinal multidrug resistance, and adaptive immunity. However, numerous physiological roles of bile acids remain undetermined. In this study, we solved the crystal structure of human serine hydroxymethyltransferase (hSHMT) in complex with an endogenous secondary bile acid glycine conjugate. The specific interaction between hSHMT and the ligand was demonstrated using mutational analyses, biophysical measurements, and structure-activity relationship studies, suggesting that secondary bile acid conjugates may act as modulators of SHMT activity.

INTRODUCTION

Bile acids, the abundant organic compounds in human bile, are synthesized via cytochrome P450-mediated oxidation of cholesterol. Bile acid pools differ greatly among biological species, and even among mammals. Humans possess five main types of bile acids: cholic acid (CA), chenodeoxycholic acid (CDCA), deoxycholic acid (DCA), ursodeoxycholic acid (UDCA), and lithocholic acid (LCA) (Figure 1A).

Figure 1B shows bile acid metabolism. CA and CDCA, called primary bile acids, are the most abundant species in the liver. Bile acids are normally transported in glycine- or taurine-conjugated state. The conjugation reaction is catalyzed by bile acid-CoA synthetase (BACS) and bile acid-CoA:amino acid *N*-acyltransferase (BAT) (Falany et al., 1994). Primary bile acids (CA and CDCA) promote lipid digestion by digestive systems, and they are transported into the intestine as glycocholic acid (Gly-CA) and taurocholic acid (Tau-CA), or as glycochenodeoxycholic acid (Gly-CDCA) and taurochenodeoxycholic acid (Tau-CDCA), respectively. In the intestine, glycine- or taurine-conjugated primary bile acids are released by bile salt hydrolase (BSH) to regenerate CA and CDCA (Begley et al., 2006). Portions of CA and CDCA are transformed into DCA, UDCA, and LCA by the elimination or configurational inversion of a hydroxyl group at the sterol moiety. These conversions are catalyzed by intestinal bacteria, and DCA, UDCA, and LCA are called secondary bile acids. Only 5% of the intestinal bile acid pool is excreted as feces, whereas the remaining 95% of the bile acid pool is transported back into the liver. Part of secondary bile acids are supposed to be conjugated using glycine or taurine as glycodeoxycholic acid (Gly-DCA) and taurodeoxycholic acid (Tau-DCA), as glycoursodeoxycholic acid (Gly-UDCA) and tauroursodeoxycholic acid (Tau-UDCA), or as glycolithocholic acid (Gly-LCA) and taurolithocholic acid (Tau-LCA), respectively.

Bile acids act as supplementary molecules, promoting lipid digestion and absorption. Recent studies have shown that bile acids also play crucial roles in regulating various biological events. For example, bile acids can act as endogenous agonists against farnesoid X receptor (FXR) (Makishima et al., 1999; Wang et al., 1999; Parks et al., 1999). Bile acid-mediated activation of FXR regulates the expression of a specific cytochrome P450, the rate-determining enzyme in bile acid biosynthesis (Sinal et al., 2000), and that of bile acid transporters (Ananthanarayanan et al., 2001). TGR5, one of the G protein-coupled receptors, was also identified as a cell-surface bile acid receptor (Kawamata et al., 2003). Through TGR5 activation, bile acids also regulate various physiological phenomena (Duboc et al., 2014; Deutschmann et al., 2018). Furthermore, bile acids regulate glucose metabolism (Stayrook et al., 2005; Zhang et al., 2006) and

[1]Department of Chemistry and Biotechnology, Graduate School of Engineering, The University of Tokyo, 7-3-1 Hongo, Bunkyo-ku, Tokyo, 113-8656, Japan

[2]Graduate School of Life Science, University of Hyogo, 3-2-1 Kouto, Kamigori-cho, Ako-gun, Hyogo, 678-1297, Japan

[3]ROD (Single Crystal Analysis) Group, Application Laboratories, Rigaku Corporation, 3-9-12 Matsubara-cho, Akishima, Tokyo, 196-8666, Japan

[4]RIKEN SPring-8 Center, 1-1-1 Kouto, Sayo-cho, Sayo-gun, Hyogo, 679-5148, Japan

[5]Institute of Medical Science, The University of Tokyo, 4-6-1, Shirokanedai, Minato-ku, Tokyo, 108-8639, Japan

[6]Department of Bioengineering, Graduate School of Engineering, The University of Tokyo, 7-3-1, Hongo, Bunkyo-ku, Tokyo 113-8656, Japan

[7]These authors contributed equally.

[8]Lead contact

*Correspondence: ssando@chembio.t.u-tokyo.ac.jp

https://doi.org/10.1016/j.isci.2021.102036

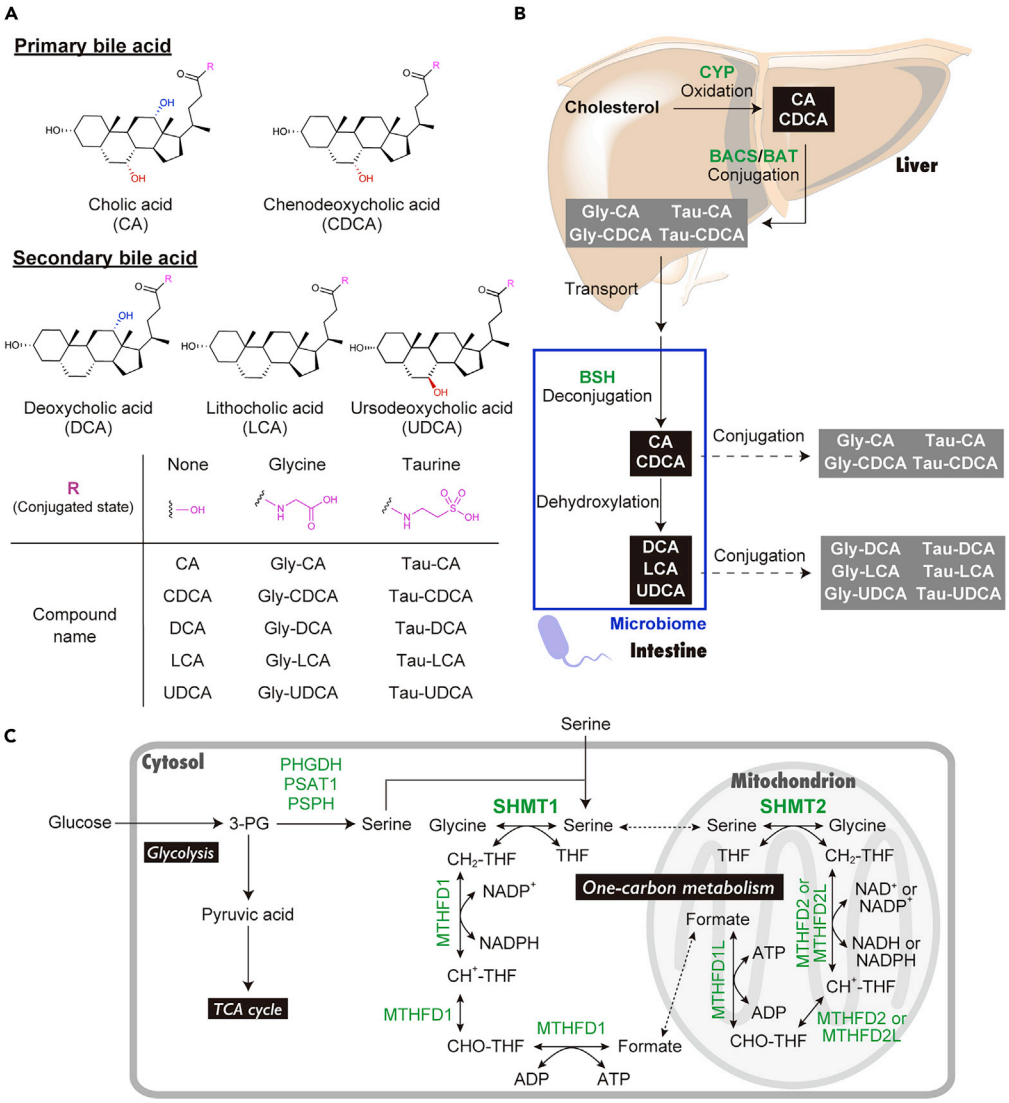

Figure 1. Human bile acid metabolism and one-carbon metabolism

(A) Chemical structures of human bile acids.

(B) Schematic illustration of bile acid metabolism. CYP = cytochrome P450, BACS = bile acid-CoA synthetase, BAT = bile acid CoA-amino acid *N*-acyltransferase, BSH = bile salt hydrolase.

(C) Schematic illustration of cellular one-carbon metabolism. 3-PG = 3-phosphoglycerate, PHGDH = phosphoglycerate dehydrogenase, PSAT1 = phosphoserine aminotransferase 1, PSPH = phosphoserine phosphatase, SHMT = serine hydroxymethyltransferase, MTHFD = methylenetetrahydrofolate dehydrogenase-cyclohydrolase, CH_2-THF = *N*-5, *N*-10-methylenetetrahydrofolate, CH^+-THF = 5,10-methenyltetrahydrofolate, CHO-THF = 10-formyltetrahydrofolate, $NADP^+$ = nicotinamide adenine dinucleotide phosphate, NADPH = $NADP^+$ reduced form.

modulate RORγ$^+$ regulatory T cell homeostasis (Song et al., 2020). Recent studies have shown that bile acids also play roles in the intestinal microbiome. For example, X-ray crystallography suggests that bile acids work as modulators of multidrug resistance in intestinal bacteria (Yamasaki et al., 2019). These physiological roles of bile acids have been garnering attention in the research community.

Herein, we successfully solved the complex structure of human serine hydroxymethyltransferase (hSHMT) and Gly-DCA at a sufficient resolution and elucidated the unique inhibitory mechanism involved in Gly-DCA-mediated inhibition of hSHMT. We also verified the specific interaction between Gly-DCA and hSHMT using a series of mutational studies, biophysical measurements, and structure-activity relationship studies. We further evaluated the inhibitory activity of 15 human bile acids against hSHMT and discovered

that Gly/Tau conjugates of secondary bile acids LCA/DCA, especially Gly-LCA and Gly-DCA, efficiently inhibit the activity of hSHMT.

SHMT is one of the key enzymes in cellular one-carbon metabolism (Figure 1C). hSHMT has two isoforms: hSHMT1 and hSHMT2. hSHMT1 is localized in the cytosol, whereas hSHMT2 is localized in the mitochondria and also in the cytosol as SHMT2α (Giardina et al., 2015). One-carbon metabolism, which is branched from glycolysis via the serine synthesis pathway, transfers the one-carbon unit derived from serine to multiple biochemical pathways such as nucleotide biosynthesis, amino acid homeostasis, redox balance, and epigenetic regulation (Locasale, 2013). Therefore, one-carbon metabolism is pivotal in maintaining cellular functions. The observed interaction between SHMT and bile acids implies that bile acid metabolites may work as endogenous modulators of one-carbon metabolism.

RESULTS

Crystal structure of hSHMT bile acid glycine conjugate complex

In our previous study, we performed high-throughput screening of inhibitors targeting hSHMT1 utilizing a fluorescent molecular probe for monitoring hSHMT activity (Nonaka et al., 2019); we obtained two specific candidate inhibitors of hSHMT, one of which was glycodeoxycholic acid (Gly-DCA). In this study, we successfully obtained the crystal of hSHMT bound with Gly-DCA. Specifically, the crystal structure of hSHMT1 in complex with Gly-DCA (Figure 2A) was solved using a soaking method at a resolution of 3.1/3.7 Å, because the crystals of hSHMT1 diffracted anisotropically to 3.1 Å in the best direction, and about 3.7 Å in the worst direction; the co-crystal structure of hSHMT2–Gly-DCA complex (Figure 3A) was solved at a resolution of 2.3 Å. SHMT was displayed in a dimeric state, the minimum oligomeric unit that constitutes the active site. The electron density corresponding to Gly-DCA is displayed as a mesh in Figures 2B and 3B. Refinement statistics are shown in Tables S1, S2, and Figure S1. SHMT is a PLP (pyridoxal 5′-phosphate)-dependent enzyme. Because PLP catalyzes the transfer of a hydroxymethyl group in the serine-glycine interconversion mediated by SHMT, PLP exists in the active site of SHMT. Crystal structure suggests that Gly-DCA is located near PLP and occludes the substrate pocket of hSHMT (Figures 2A, 2B, 3A, and 3B).

As illustrated in Figures 2B and 3B, many interactions seem to be formed between hSHMT and Gly-DCA (2D interaction maps were shown in Figures S4 and S5). Among protein-ligand non-covalent bonding, putative hydrogen bonding and salt bridge were illustrated as red dotted line and black dotted line, respectively. Electrostatic interactions seem to be formed mainly in the conjugated glycine moiety of Gly-DCA (Figures 2B and 3B). The amide group of Gly-DCA is recognized by Arg402 in hSHMT1, or by Glu98 and Arg425 in hSHMT2. The carboxylic acid group of Gly-DCA is recognized by Ser53 and PLP in hSHMT1, or by Ser226 and Arg425 in hSHMT2. Glu75 and Arg402 in hSHMT1, which correspond to Glu98 and Arg425 in hSHMT2, play crucial roles in substrate recognition and catalysis of Ser-Gly conversion (Jagath et al., 1997; Szebenyi et al., 2004; Schirch and Szebenyi, 2005) (Figure S6). X-ray crystallography for hSHMT2 suggests that the conjugated glycine moiety of Gly-DCA formed hydrogen bond with Glu98 and a salt bridge with Arg425 in hSHMT2 (Figure 3B), whereas crystal structure of hSHMT1 complexed with Gly-DCA suggests that Gly-DCA contacted with Glu75 and amide group of Gly-DCA formed a hydrogen bond with Arg402 (Figure 2B). Our result indicates that these interactions of Glu and Arg with Gly-DCA contributed to the effective inhibition of hSHMT activity.

To support the data indicated by the aforementioned X-ray crystallographic analysis, we further conducted a mutational study of hSHMT1 and hSHMT2 based on binding affinity analysis. hSHMT1 or hSHMT2 mutants, hSHMT1 E75L and hSHMT1 R402A or hSHMT2 E98L and hSHMT2 R425A were generated by substituting hydrophobic residues for polar residues. To evaluate binding affinity, we used surface plasmon resonance to measure the dissociation constant (K_d) of Gly-DCA for wild-type (WT) or mutant hSHMT at 25°C. The K_d of Gly-DCA for hSHMT1 WT was 7.6 μM, whereas that for hSHMT1 E75L was 73.5 μM; the binding affinity of Gly-DCA for hSHMT1 R402A was too weak to quantitate (Figure S7). The K_d of Gly-DCA for hSHMT2 WT was 0.064 μM, whereas the binding affinity of Gly-DCA for hSHMT2 E98L or R425A was too weak to quantitate (Figure S8). These results show that these hSHMT1 and 2 mutants displayed greatly decreased binding affinity for Gly-DCA. Circular dichroism measurements revealed that these hSHMT mutants showed nearly the same spectra and intensity as those of hSHMT WT (Figure S9), suggesting that these mutations did not disturb the secondary structure of hSHMT. This indicates that the decreased binding affinity was not caused by denaturation of the entire protein, and that local contributions from the amino acid residues of interest in hSHMT were important for the interaction with Gly-DCA. These results

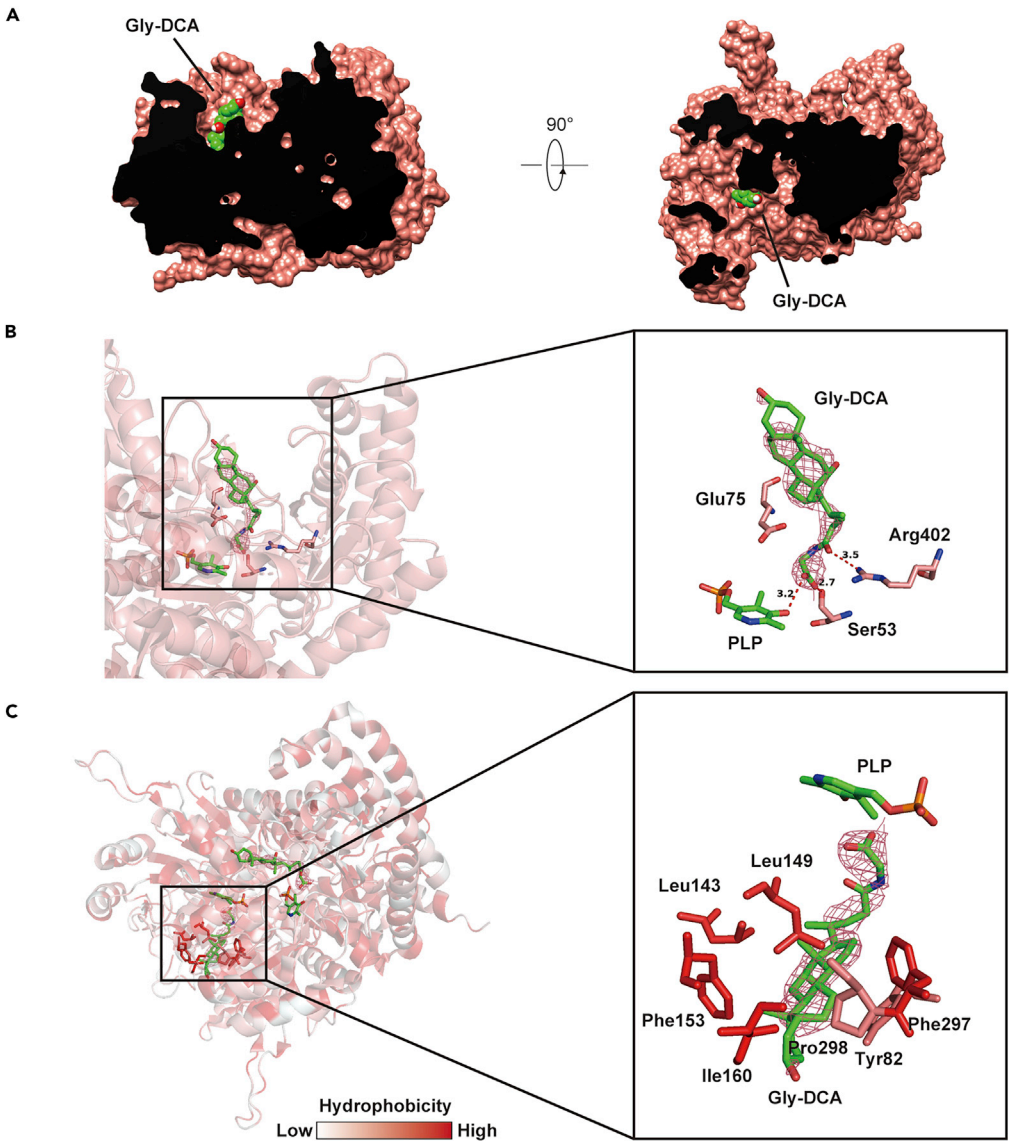

Figure 2. Crystal structure of hSHMT1-Gly-DCA complex

(A) Surface representation of the hSHMT1 dimer from two different perspectives. Gly-DCA is displayed as spherical model with carbon shown in green.

(B) Interaction between hSHMT1 and Gly-DCA. Gly-DCA is shown as a stick model with carbon in green, whereas hydrogen bonding is represented as red dotted line. 2mFo-DFc electron density of Gly-DCA at the contour level 1.0 σ is shown as a raspberry mesh. Polder map version is shown in Figure S2A.

(C) Protein mapping of hSHMT1 using the Eisenberg hydrophobic scale. Polder map version is shown in Figure S2B.

also indicate that the polar residues, Arg402 in hSHMT1 or Glu98 and Arg425 in hSHMT2, were important residues for the interactions with the conjugated glycine moiety of Gly-DCA by hSHMT1 or hSHMT2.

Next, we analyzed the interactions between the sterol moiety of Gly-DCA and hSHMT. Because of its high hydrophobicity, the sterol moiety of a bile acid is more suitable for hydrophobic or CH/π interactions than for electrostatic interactions. In Figures 2C and 3C, the hydrophobicity of hSHMT is shown as a heatmap. The hydrophobicity of each amino acid residue was colored following the Eisenberg hydrophobic scale (Eisenberg et al., 1984) in which color depth of protein surface represents the degree of hydrophobicity. As shown in Figures 2C and 3C (Figures S4 and S5), the sterol moiety of Gly-DCA seems to interact with hydrophobic residues of hSHMT (hSHMT1: Tyr82, Leu143, Leu149, Phe153, Ile160, Phe297, and Pro298; hSHMT2: Tyr105, Leu166, Leu172, Tyr176, Ile183, Phe320,

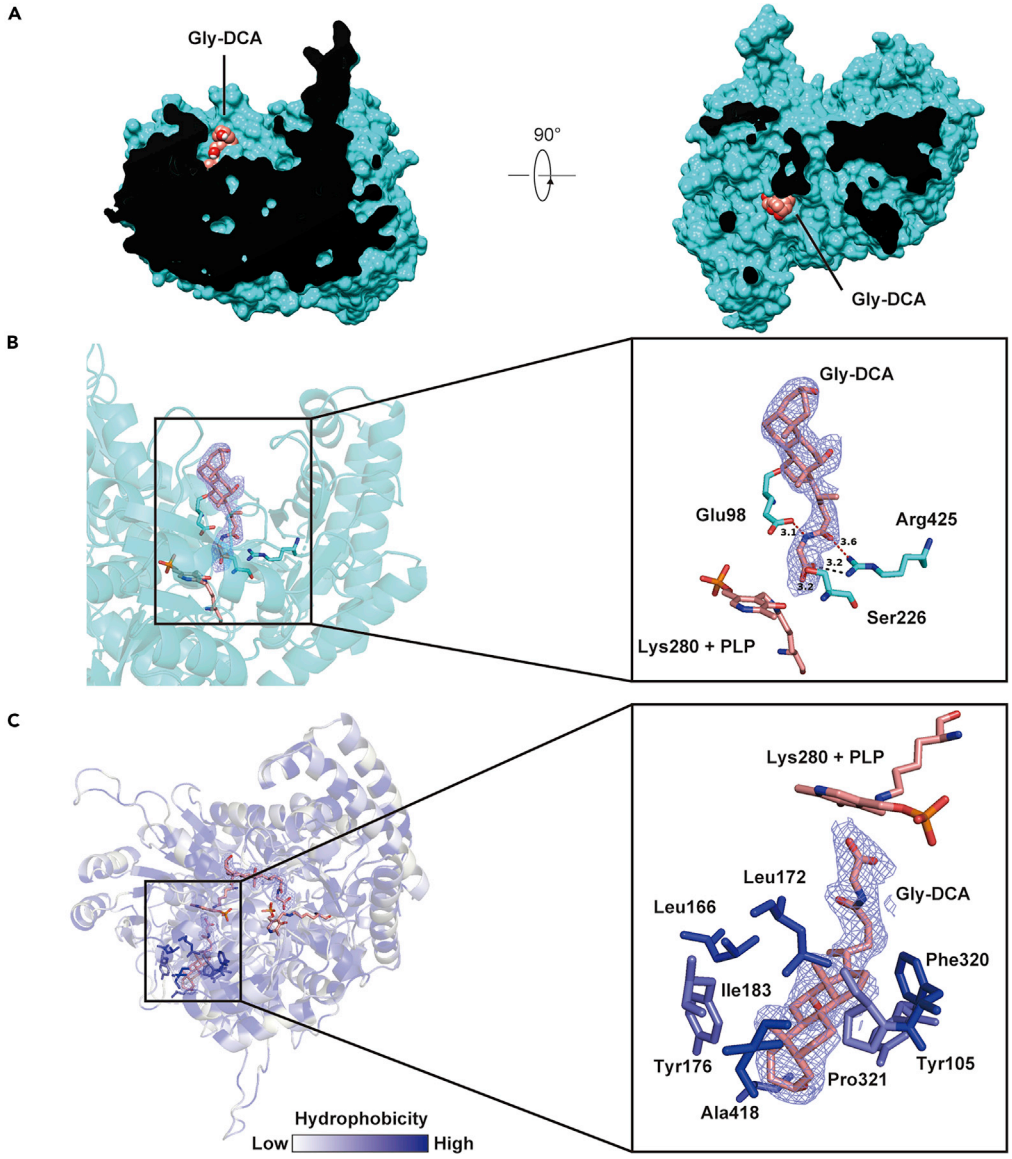

Figure 3. Crystal structure of hSHMT2-Gly-DCA complex

(A) Surface representation of the hSHMT2 dimer from two different perspectives. Gly-DCA is shown as a spherical model with carbon displayed in salmon.

(B) Interaction between hSHMT2 and Gly-DCA. Gly-DCA is shown as a stick model with carbon displayed in salmon, whereas hydrogen bonding and salt bridge are represented as red dotted line and black dotted line, respectively. 2mFo-DFc electronic density of Gly-DCA at the contour level 1.0 σ is displayed as purple mesh. Polder map version is shown in Figure S3A.

(C) Protein mapping of hSHMT2 using the Eisenberg hydrophobic scale. Polder map version is shown in Figure S3B.

Pro321, and Ala418). These interactions included not only a broad range of hydrophobic interactions but also multiple CH/π interactions, e.g., Tyr82 and Phe153 in hSHMT1 and Tyr105 and Ty176 in hSHMT2, which contributed to enthalpic stabilization. In summary, the efficient binding of Gly-DCA with hSHMT was driven by the synergetic effect of electrostatic interaction in the glycine moiety and hydrophobic and CH/π interaction in the sterol moiety.

Energetic basis for protein-ligand interaction

We used isothermal titration calorimetry (ITC) and differential scanning calorimetry (DSC) to verify that Gly-DCA specifically bound with hSHMT (Figure 4).

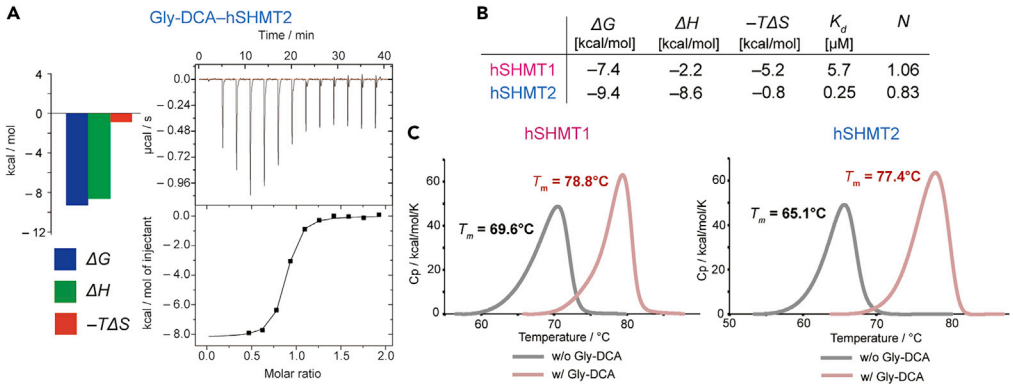

	ΔG [kcal/mol]	ΔH [kcal/mol]	−TΔS [kcal/mol]	K_d [µM]	N
hSHMT1	−7.4	−2.2	−5.2	5.7	1.06
hSHMT2	−9.4	−8.6	−0.8	0.25	0.83

Figure 4. Energetic basis for hSHMT-Gly-DCA interactions

(A) The binding of hSHMT2 with Gly-DCA assessed using isothermal titration calorimetry (ITC). ITC was conducted at 37°C in 10 mM HEPES pH 7.5, 200 mM NaCl, 0.5 mM EDTA, 2 mM β-mercaptoethanol, 50 µM PLP, and 3% (v/v) DMSO.

(B) ITC profiles of hSHMT1-Gly-DCA and hSHMT2-Gly-DCA interactions. Calorimetric data for hSHMT1 were obtained from our previous report (Nonaka et al., 2019).

(C) The binding of Gly-DCA with hSHMT1 or hSHMT2 assessed using differential scanning calorimetry (DSC). DSC was conducted at the speed of 1°C/min in 10 mM HEPES pH 7.5, NaCl (100 mM for hSHMT1 and 200 mM for hSHMT2), 0.5 mM EDTA, 2 mM β-mercaptoethanol, 50 µM PLP (used only for hSHMT2), 18 µM hSHMT1 or hSHMT2 (1.0 mg/mL each), 50 µM Gly-DCA, and 1% (v/v) DMSO. The concentrations of salt and PLP differed slightly for hSHMT1 (100 mM NaCl and 0 µM PLP) and hSHMT2 (200 mM NaCl and 50 µM PLP). This is because hSHMT2 tends to aggregate and release PLP under the conditions used for hSHMT1.

We used ITC to quantitatively evaluate the interactions between Gly-DCA and hSHMT. Using ITC, we analyzed the thermodynamic profile of energetic stabilization during the binding of a ligand with a protein. We previously determined that the binding of Gly-DCA with hSHMT1 is driven by both enthalpic and entropic stabilization (Nonaka et al., 2019). Thermodynamic parameters are shown in Figure 4B (ΔG = −7.4 kcal/mol, ΔH = −2.2 kcal/mol, $-T\Delta S$ = −5.2 kcal/mol, K_d = 5.7 µM). In our present study, we measured the binding profile of Gly-DCA with hSHMT2 using ITC and obtained the thermodynamic parameters of: ΔG = −9.4 kcal/mol, ΔH = −8.6 kcal/mol, $-T\Delta S$ = −0.8 kcal/mol, and K_d = 0.25 µM (Figures 4A and 4B). Comparison of the dissociation constant value obtained in our previous study with that obtained in our current study indicated that Gly-DCA binds more tightly with hSHMT2 (K_d = 0.25 µM) than with hSHMT1 (K_d = 5.7 µM). We also found that the binding of Gly-DCA with hSHMT2 was driven mainly by enthalpic stabilization. Furthermore, the stoichiometry (binding ratio) was N = 1.06 in hSHMT1 and N = 0.83 in hSHMT2, which is close to N = 1 (Figure 4B). This indicates that one molecule of Gly-DCA bound with a monomer of hSHMT.

Next, we used DSC to further evaluate the interactions between Gly-DCA and hSHMT. In DSC, the thermal stability of a protein can be evaluated using melting temperature (T_m) as an indicator. We evaluated changes in the thermal stability of hSHMT during the addition of Gly-DCA. Our results show that Gly-DCA induced a significant increase in the thermal stability of both hSHMT1 (ΔT_m = 9.2°C, T_m = 69.6°C → 78.8°C) and hSHMT2 (ΔT_m = 12.3°C, T_m = 65.1°C → 77.4°C) (Figure 4C). This result was consistent with the order of binding affinity obtained by ITC.

The results of ITC and DSC validated the notion that Gly-DCA binds more tightly with hSHMT2 than with hSHMT1. This is interesting considering the active sites are well conserved and almost similar between hSHMT1 and hSHMT2. Superimposing the crystal structure of hSHMT1 complexed with Gly-DCA onto the co-crystal structure of the hSHMT2–Gly-DCA complex showed that orientation of the sterol moiety in Gly-DCA differed in each complex (Figure S10). Although it is difficult to draw precise conclusion from the comparison of these crystal structures, the high binding affinity of Gly-DCA for hSHMT2 may be due to the more robust electrostatic, hydrophobic, and CH/π interactions resulting from the different orientation of sterol moiety.

Both ITC and DSC data strongly support the notion that Gly-DCA specifically interacted with hSHMT. Because Gly-DCA bound more strongly with hSHMT2 than with hSHMT1, we used hSHMT2 to subsequently evaluate the inhibitory ability of Gly-DCA.

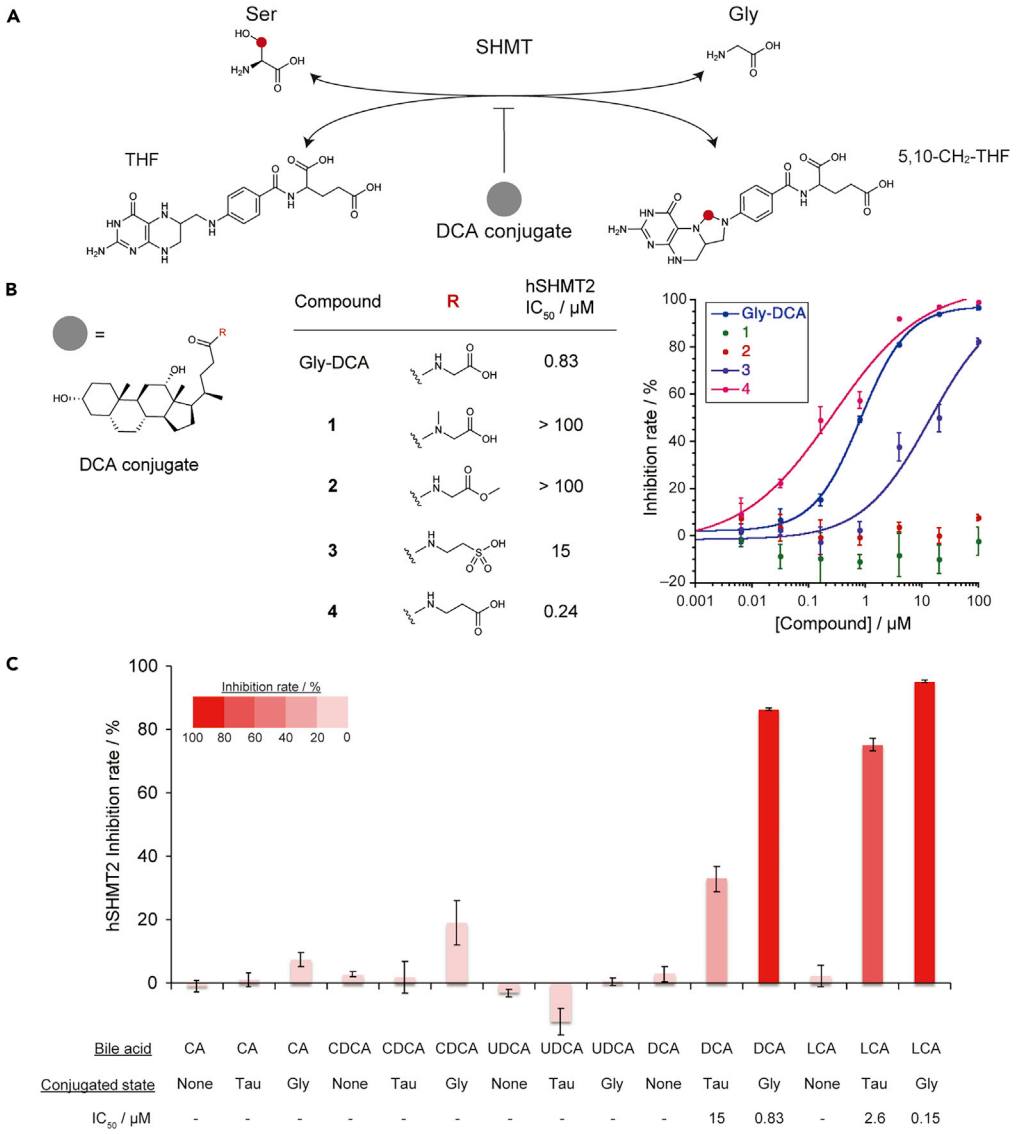

Figure 5. Structure-activity relationship

(A) Serine-glycine conversion catalyzed by SHMT. THF = tetrahydrofolate, 5,10-CH_2-THF = *N*-5, *N*-10-methylenetetrahydrofolate. The carbon atom that is transferred from Ser to THF is shown as red dot.

(B) Structure expansion for the bile acid conjugate moiety. Assay conditions: 10 mM HEPES pH 7.5, 100 mM NaCl, 0.5 mM EDTA, 1 mM DTT, 1 mM L-Ser, 0.2 mM THF, 1% (v/v) DMSO. Error bars represent SD, $n = 3$.

(C) Heatmap and bar graph representing the inhibitory effect of human bile acids against hSHMT2. Assay conditions: 10 mM HEPES pH 7.5, 100 mM NaCl, 0.5 mM EDTA, 1 mM DTT, 1 mM L-Ser, 0.2 mM THF, 5 μM compound, 1% (v/v) DMSO. Error bars represent SD, $n = 3$. IC_{50} values by Gly/Tau-DCA and Gly/Tau-LCA are shown below the bar graph.

Structure-activity relationship between Gly-DCA and hSHMT2

We next conducted a structure-activity relationship analysis of the interactions between Gly-DCA and hSHMT2. SHMT catalyzes the serine-glycine interconversion in conjunction with tetrahydrofolate (THF) and *N*-5,*N*-10-methylenetetrahydrofolate (5,10-CH_2-THF) (Figure 5A). The half-maximal inhibitory concentration (IC_{50}) was used to evaluate inhibitory activity in this enzymatic reaction.

If polar functional groups of Gly-DCA are recognized by hSHMT, masking the exchangeable proton in the amide or carboxylic acid group of Gly-DCA would be expected to weaken the inhibitory activity. We synthesized compound 1 (in which a secondary amide group of Gly-DCA was transformed into a tertiary

N-methyl amide group) and compound 2 (in which a carboxylic acid group of Gly-DCA was esterified by methylation) (Figure 5B). We previously showed that Gly-DCA inhibits the enzymatic reaction catalyzed by hSHMT (Nonaka et al., 2019). The IC_{50} value for Gly-DCA against hSHMT2 was 0.83 μM. Under the same experimental conditions, the IC_{50} values of compounds 1 and 2 exceeded 100 μM. These results indicate that local polarity was important for specific recognition by hSHMT (Figure 5B).

We next used taurodeoxycholic acid (Tau-DCA, compound 3) to further evaluate the structure-activity relationship with respect to Gly-DCA. The IC_{50} value of 15 μM for Tau-DCA against hSHMT2 indicated a decrease in the inhibitory effects compared with Gly-DCA (Figure 5B). The difference in the inhibitory activity of Gly-DCA and Tau-DCA was likely due to the difference in the number of carbon atoms or functional groups. To evaluate spatial capacity, we synthesized compound 4 in which the glycine moiety of Gly-DCA was transformed into a β-alanine moiety. The IC_{50} value of compound 4 against hSHMT2 was 0.24 μM, indicating that it exerted an inhibitory activity that was stronger than that of Gly-DCA (Figure 5B). This indicates that there was sufficient space to accommodate an additional carbon atom on the conjugated glycine moiety of Gly-DCA in the deep site of the substrate pocket of hSHMT2. Therefore, the reduced inhibitory effect for Tau-DCA is likely derived from differences in the properties of carboxylic acid group and sulfonic acid group. These results indicate that the conjugated glycine of Gly-DCA was specifically recognized by hSHMT by electrostatic interactions such as hydrogen bonding and salt bridge, leading to high inhibitory activity.

We investigated the mechanism of inhibition at the enzyme's active site (Scaletti et al., 2019). Comparison of the hSHMT2-Gly-DCA structure with apo hSHMT2 (PDB ID: 4PVF) suggests that the majority of amino acid residues within the active site maintained the same positions upon ligand binding, whereas Tyr105 and Tyr106 moved drastically (Giardina et al., 2015) (Figure S11).

Evaluation of inhibitory activity of human bile acids against hSHMT

In humans, five core bile acids (CA, DCA, CDCA, UDCA, LCA) are metabolically synthesized from cholesterol (Figures 1A and 1B). Humans possess mainly 15 types of bile acids, including glycine and taurine conjugates of each bile acid core (CA, DCA, CDCA, UDCA, LCA, Gly-CA, Gly-DCA, Gly-CDCA, Gly-UDCA, Gly-LCA, Tau-CA, Tau-DCA, Tau-CDCA, Tau-UDCA, Tau-LCA) (Figure 1A). Gly-DCA selectively interacts with hSHMT and inhibits its activity. Considering the structural similarity among bile acid cores, we assumed that other bile acids also inhibit hSHMT activity. Therefore, we evaluated the inhibitory effects of 15 types of bile acids against hSHMT2, which are shown as a heatmap and bar graph in Figure 5C. Interestingly, among various bile acids and their conjugates having nearly identical structures, secondary bile acid conjugates (Gly-DCA, Gly-LCA, Tau-DCA, Tau-LCA) showed stronger inhibitory effects against hSHMT2 than those of primary bile acids (CA and CDCA) and their conjugates (Gly-CA, Gly-CDCA, Tau-CA, Tau-CDCA) or those of secondary bile acids (DCA, LCA, UDCA) and their conjugates (Gly-UDCA and Tau-UDCA). Furthermore, we quantitatively evaluated the inhibitory activity of secondary bile acid conjugates against hSHMT2. The IC_{50} values of Gly-DCA, Gly-LCA, Tau-DCA, and Tau-LCA were 0.83, 0.15, 15, and 2.6 μM, respectively (Figures 5B and S12), suggesting that secondary bile acid glycine conjugates (Gly-DCA and Gly-LCA) showed particularly strong inhibitory effects against hSHMT2 (Figure 5C).

Glycine-conjugated secondary bile acids showed relatively stronger inhibitory effects against hSHMT than those of deconjugated or taurine-conjugated secondary bile acids. As shown in Figure 3B, the amide and carboxylic acid groups of Gly-DCA formed electrostatic interactions with the polar residues of hSHMT, such as hydrogen bonding or salt bridge, whereas the sterol moiety of Gly-DCA formed hydrophobic and CH/π interactions with the non-polar residues of hSHMT. Deconjugated bile acids bearing a sterol moiety are expected to bind to hSHMT by hydrophobic and CH/π interactions. However, deconjugated bile acids cannot form strong electrostatic interactions because of the absence of the amide and carboxylic acid group derived from the conjugated glycine, which leads to weak binding and reduced inhibition against hSHMT. Secondary bile acids in a taurine-conjugated state showed relatively weak inhibitory effects against hSHMT. This was likely due to differences in the properties of carboxylic acid group and sulfonic acid group, as shown in Figure 5B.

DISCUSSION

In this study, we successfully solved the crystal structure of hSHMT in complex with Gly-DCA at a resolution (hSHMT1Gly-DCA: 3.1/3.7 Å; hSHMT2–Gly-DCA: 2.3 Å). A mutational study based on X-ray crystallography

was used to validate the interaction between Gly-DCA and hSHMT. Biophysical measurements, such as ITC and DSC, revealed the specific binding manner between Gly-DCA and hSHMT. Structure-activity relationship studies for Gly-DCA showed that Gly-DCA specifically inhibited the activity of hSHMT. Gly/Tau-conjugates of secondary bile acids, especially Gly-LCA and Gly-DCA, showed particularly strong inhibitory effects against hSHMT.

Bile acids function as innate detergents and play physiological roles in the regulation of their own metabolism (Sinal et al., 2000; Ananthanarayanan et al., 2001), glucose metabolism (Stayrook et al., 2005; Zhang et al., 2006), adaptive immunity (Song et al., 2020), and multidrug resistance in intestinal bacteria (Yamasaki et al., 2019). To the best of our knowledge, this study is the first to reveal that endogenous secondary bile acid conjugates specifically interacted with, and inhibited the activity of, hSHMT. SHMT is an enzyme that catalyzes the serine-glycine conversion and serves as a starting point for cellular one-carbon metabolism. One-carbon metabolism is involved in the synthesis of biological molecules requisite for cell division and proliferation, including nucleotide biosynthesis (Locasale, 2013). SHMT also plays physiologically important roles in the regulation of tRNA modification (Asano et al., 2018; Minton et al., 2018; Morscher et al., 2018) and the immune response (Walden et al., 2019). For these reasons, SHMT has attracted increasing attention as a target (Jain et al., 2012; Paone et al., 2014; Gupta et al., 2017; Woo et al., 2016; Kim et al., 2015) in drug development (Dekhne et al., 2019, 2020; Ducker et al., 2017).

The results of our present study suggest that endogenous secondary bile acid conjugates may work as regulators of one-carbon metabolism, because they can modulate the key SHMT activity. Although these are beyond the scope of this study, the observed specific interactions between SHMT and secondary bile acid conjugates imply that bile acids play numerous and still undiscovered roles.

Limitations of the study

The data presented has revealed the specific interaction of hSHMT with secondary bile acid conjugates. However, it should be noted that these results do not directly prove the intracellular interaction. Further biochemical studies are needed to prove the interaction in cells, and further biological studies are needed to clarify the potential physiological role of bile acid conjugates as SHMT inhibitors or modulators.

Resource availability

Lead contact

Further information and requests for resources and materials should be directed to and will be fulfilled by the Lead Contact, Shinsuke Sando (ssando@chembio.t.u-tokyo.ac.jp).

Material availability

Materials are available upon reasonable request.

Data and code availability

Crystal structures of hSHMT1 and hSHMT2 with Gly-DCA have been deposited in the Protein DataBank under the following accession codes, PDB: 6M5W and PDB: 6M5O, respectively.

METHODS

All methods can be found in the accompanying Transparent methods supplemental file.

SUPPLEMENTAL INFORMATION

Supplemental information can be found online at https://doi.org/10.1016/j.isci.2021.102036.

ACKNOWLEDGMENTS

S.S. acknowledges financial support from CREST (JPMJCR13L4), Japan Science and Technology Agency, and partly from JSPS KAKENHI (19H00919). K.T. acknowledges financial support from JSPS (JP19H05766 and JM16H02420). S.N. acknowledges financial support from JSPS (JP18H02082). This research was supported by Platform Project for Supporting Drug Discovery and Life Science Research (Basis for Supporting Innovative Drug Discovery and Life Science Research (BINDS)) from AMED (JP19am0101001 and JP19am0101094). We thank the staffs of the SPring-8 (BL26B2) for excellent technical support. Plasmid

for recombinant hSHMT2 including A269T mutation was a gift from Prof. C. Arrowsmith of University of Toronto, Canada (Addgene plasmid # 25479).

AUTHOR CONTRIBUTIONS

H.N. and S.S. conceived and designed the project. T.O., A.S., S.I., G.U., S.N., and K.T. performed X-ray crystallographic analysis. T.O., M.S., and Y.S. performed synthesis of bile acids. T.O. and M.S. performed the mutational studies, biophysical measurements, and structure-activity relationship studies with support from A.S., S.N., and K.T. The manuscript was written by T.O. and S.S. and edited by all the coauthors.

DECLARATION OF INTERESTS

The authors declare no competing interests.

Received: November 5, 2020
Revised: December 8, 2020
Accepted: December 31, 2020
Published: February 19, 2021

REFERENCES

Ananthanarayanan, M., Balasubramanian, N., Makishima, M., Mangelsdorf, D.J., and Suchy, F.J. (2001). Human bile salt export pump promoter is transactivated by the farnesoid X receptor/bile acid receptor. J. Biol. Chem. *276*, 28857–28865.

Asano, K., Suzuki, T., Saito, A., Wei, F.-Y., Ikeuchi, Y., Numata, T., Tanaka, R., Yamane, Y., Yamamoto, T., Goto, T., et al. (2018). Metabolic and chemical regulation of tRNA modification associated with taurine deficiency and human disease. Nucleic Acids Res. *46*, 1565–1583.

Begley, M., Hill, C., and Gahan, C.G.M. (2006). Bile salt hydrolase activity in probiotics. Appl. Environ. Microbiol. *72*, 1729–1738.

Deutschmann, K., Reich, M., Klindt, C., Dröge, C., Spomer, L., Häussinger, D., and Keitel, V. (2018). Bile acid receptors in the biliary tree: TGR5 in physiology and disease. Biochim. Biophys. Acta Mol. Basis Dis. *1864*, 1319–1325.

Dekhne, A.S., Ning, C., Nayeen, J., Shah, K., Kalpage, H., Frühauf, J., Wallace-Povirk, A., O'Connor, C., Hou, Z., Kim, S., et al. (2020). Cellular pharmacodynamics of a novel pyrrolo [3,2-d]pyrimidine inhibitor targeting mitochondrial and cytosolic one-carbon metabolism. Mol. Pharmacol. *97*, 9–22.

Dekhne, A.S., Shah, K., Ducker, G.S., Katinas, J.M., Wong-Roushar, J., Nayeen, J., Doshi, A., Ning, C., Bao, X., Frühauf, J., et al. (2019). Novel pyrrolo[3,2-d]pyrimidine compounds target mitochondrial and cytosolic one-carbon metabolism with broad-spectrum antitumor efficacy. Mol. Cancer Ther. *18*, 1787–1799.

Duboc, H., Taché, Y., and Hofmann, A.F. (2014). The bile acid TGR5 membrane receptor: From basic research to clinical application. Dig. Liver Dis. *46*, 302–312.

Ducker, G.S., Ghergurovich, J.M., Mainolfi, N., Suri, V., Jeong, S.K., Li, S.H.-J., Friedman, A., Manfredi, M.G., Gitai, Z., Kim, H., et al. (2017). Human SHMT inhibitors reveal defective glycine import as a targetable metabolic vulnerability of diffuse large B-cell lymphoma. Proc. Natl. Acad. Sci. U S A *114*, 11404–11409.

Eisenberg, D., Schwarz, E., Komaromy, M., and Wall, R. (1984). Analysis of membrane and surface protein sequences with the hydrophobic moment plot. J. Mol. Biol. *179*, 125–142.

Falany, C.N., Johnson, M.R., Barnes, S., and Diasio, R.B. (1994). Glycine and taurine conjugation of bile acids by a single enzyme. J. Biol. Chem. *269*, 19375–19379.

Giardina, G., Brunotti, P., Fiascarelli, A., Cicalini, A., Costa, M.G.S., Buckle, A.M., di Salvo, M.L., Giorgi, A., Marani, M., Paone, A., et al. (2015). How pyridoxal 5′-phosphate differentially regulates human cytosolic and mitochondrial serine hydroxymethyltransferase oligomeric state. FEBS J. *282*, 1225–1241.

Gupta, R., Yang, Q., Dogra, S.K., and Wajapeyee, N. (2017). Serine hydroxymethyl transferase 1 stimulates pro-oncogenic cytokine expression through sialic acid to promote ovarian cancer tumor growth and progression. Oncogene *36*, 4014–4024.

Jagath, J.R., Appaji Rao, N., and Savithri, H.S. (1997). Role of Arg-401 of cytosolic serine hydroxymethyltransferase in subunit assembly and interaction with the substrate carboxy group. Biochem. J. *327*, 877–882.

Jain, M., Nilsson, R., Sharma, S., Mandhusudhan, N., Kitami, T., Souza, A.L., Kafri, R., Kirschner, M.W., Clish, C.B., and Mootha, V.K. (2012). Metabolite profiling identifies a key role for glycine in rapid cancer cell proliferation. Science *336*, 1040–1044.

Kawamata, Y., Fujii, R., Hosoya, M., Harada, M., Yoshida, H., Miwa, M., Fukusumi, S., Habata, Y., Itoh, T., Shintani, Y., et al. (2003). A G protein-coupled receptor responsive to bile acids. J. Biol. Chem. *278*, 9435–9440.

Kim, D., Fiske, B.P., Birsoy, K., Freinkman, E., Kami, K., Possemato, R.L., Chudnovsky, Y., Pacold, M.E., Chen, W.W., Cantor, J.R., et al. (2015). SHMT2 drives glioma cell survival in ischaemia but imposes a dependence on glycine clearance. Nature *520*, 363–367.

Locasale, J.W. (2013). Serine, glycine and one-carbon units: cancer metabolism in full circle. Nat. Rev. Cancer *13*, 572–583.

Makishima, M., Okamoto, A.Y., Repa, J.J., Tu, H., Marc Learned, R., Luk, A., Hull, M.V., Lusting, K.D., Mangelsdorf, D.J., and Shan, B. (1999). Identification of a nuclear receptor for bile acids. Science *284*, 1362–1365.

Morscher, R.J., Ducker, G.S., Li, S.H.-J., Mayer, J.A., Gitai, Z., Sperl, W., and Rabinowitz, J.D. (2018). Mitochondrial translation requires folate-dependent tRNA methylation. Nature *554*, 128–132.

Minton, D.R., Nam, M., McLaughlin, D.J., Shin, J., Bayraktar, E.C., Alvarez, S.W., Sviderskiy, V.O., Papagiannakopoulos, T., Sabatini, D.M., Birsoy, K., et al. (2018). Serine catabolism by SHMT2 is required for proper mitochondrial translation initiation and maintenance of formylmethionyl-tRNAs. Mol. Cell *69*, 610–621.

Nonaka, H., Nakanishi, Y., Kuno, S., Ota, T., Mochidome, K., Saito, Y., Sugihara, F., Takakusagi, Y., Aoki, I., Nagatoishi, S., et al. (2019). Design strategy for serine hydroxymethyltransferase probes based on retro-aldol-type reaction. Nat. Commun. *10*, 876.

Paone, A., Marani, M., Fiascarelli, A., Rinaldo, S., Giardina, G., Contestabile, R., Paiardini, A., and Cutruzzolá, F. (2014). SHMT1 knockdown induces apoptosis in lung cancer cells by causing uracil misincorporation. Cell Death Dis. *5*, e1525.

Parks, D.J., Blanchard, S.G., Bledsoe, R.K., Chandra, G., Consler, T.G., Kliewer, S.A., Stimmel, J.B., Willsom, T.M., Zavacki, A.M., Moore, D.D., et al. (1999). Bile acids: natural ligands for an orphan nuclear receptor. Science *284*, 1365–1368.

Scaletti, E., Jemth, A.S., Helleday, T., and Stenmark, P. (2019). Structural basis of inhibition of the human serine hydroxymethyltransferase SHMT2 by antifolate drugs. FEBS Lett. *593*, 1863–1873.

Schirch, V., and Szebenyi, D.M. (2005). Serine hydroxymethyltransferase revisited. Curr. Opin. Chem. Biol. *9*, 482–487.

Sinal, C.J., Tohkin, M., Miyata, M., Ward, J.M., Lambert, G., and Gonzalez, F.J. (2000). Targeted disruption of the nuclear receptor FXR/BAR impairs bile acid and lipid homeostasis. Cell *102*, 731–744.

Song, X., Sun, X., Oh, S.F., Wu, M., Zhang, Y., Zheng, W., Geva-Zatorsky, N., Jupp, R., Mathis, D., Benoist, C., et al. (2020). Microbial bile acid metabolites modulate gut RORγ^{+} regulatory T cell homeostasis. Nature *577*, 410–415.

Stayrook, K.R., Bramlett, K.S., Savkur, R.S., Ficorilli, J., Cook, T., Christe, M.E., Michael, L.F., and Burris, T.P. (2005). Regulation of carbohydrate metabolism by the farnesoid X receptor. Endocrinology *146*, 984–991.

Szebenyi, D.M.E., Musayev, F.N., di Salvo, M.L., Safo, M.K., and Schirch, V. (2004). Serine hydroxymethyltransferase: role of glu75 and evidence that serine is cleaved by a retroaldol mechanism. Biochemistry *43*, 6865–6876.

Walden, M., Tian, L., Ross, R.L., Sykora, U.M., Byrne, D.P., Hesketh, E.L., Masandi, S.K., Cassel, J., George, R., Ault, J.R., et al. (2019). Metabolic control of BRISC–SHMT2 assembly regulates immune signaling. Nature *570*, 194–199.

Wang, H., Chen, J., Hollister, K., Sowers, L.C., and Forman, B.M. (1999). Endogenous bile acids are ligands for the nuclear receptor FXR/BAR. Mol. Cell *3*, 543–553.

Woo, C.C., Chen, W.C., Teo, X.Q., Radda, G.K., and Lee, P.T.H. (2016). Downregulating serine hydroxymethyltransferase 2 (SHMT2) suppresses tumorigenesis in human hepatocellular carcinoma. Oncotarget *7*, 53005–53017.

Yamasaki, S., Nakashima, R., Sakurai, K., Baucheron, S., Giraud, E., Doublet, B., Cloecksert, A., and Nishino, K. (2019). Crystal structure of the multidrug resistance regulator RamR complexed with bile acids. Sci. Rep. *9*, 177.

Zhang, Y., Lee, F.Y., Barrera, G., Lee, H., Vales, C., Gonzalez, F.J., Willson, T.M., and Edwards, P.A. (2006). Activation of the nuclear receptor FXR improves hyperglycemia and hyperlipidemia in diabetic mice. Proc. Natl. Acad. Sci. U S A *103*, 1006–1011.

iScience, Volume *24*

Supplemental Information

Structural basis for selective inhibition of human serine hydroxymethyltransferase by secondary bile acid conjugate

Tomoki Ota, Akinobu Senoo, Masumi Shirakawa, Hiroshi Nonaka, Yutaro Saito, Sho Ito, Go Ueno, Satoru Nagatoishi, Kouhei Tsumoto, and Shinsuke Sando

1. Supplemental Figures

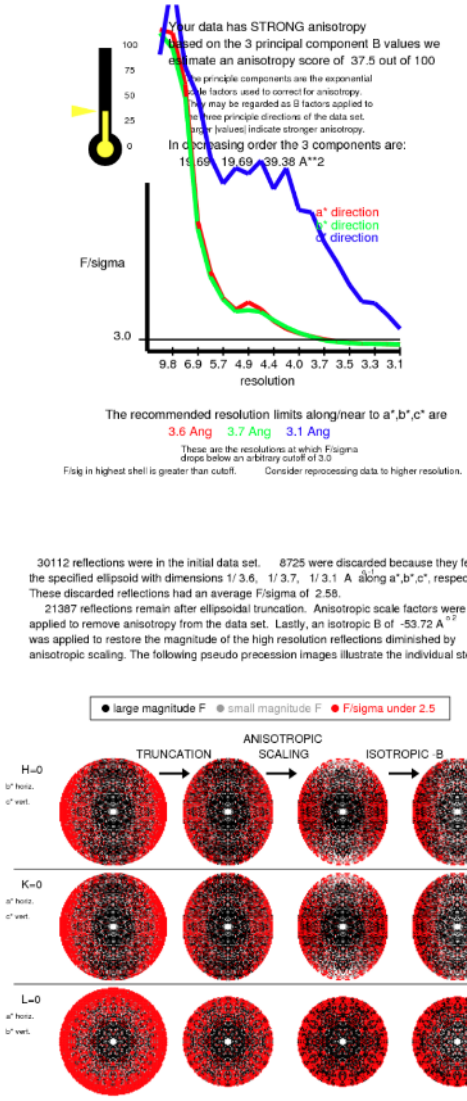

Figure S1. Results of anisotropic scaling by UCLA-MBI Diffraction Anisotropy Server, Related to Figure 2

(upper panel) Resolution limits for each reciprocal cell direction a*, b*, and c*. (lower panel) Pseudo precession images of each reciprocal cell direction a*, b*, and c* during each scaling procedure.

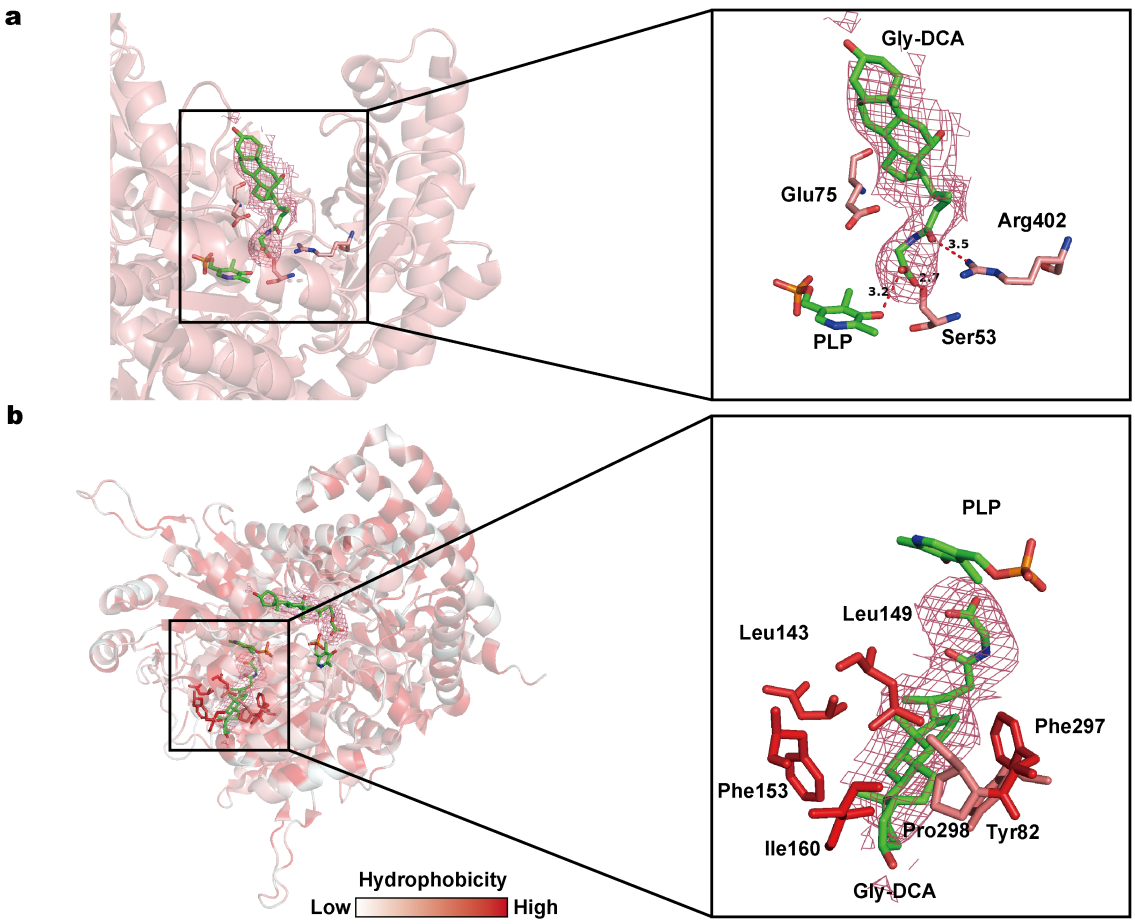

Figure S2. Crystal structure of hSHMT1–Gly-DCA complex, Related to Figure 2

a) Interaction between hSHMT1 and Gly-DCA. Gly-DCA is shown as a stick model with carbon in green. Hydrogen bonding is represented as red dotted line. Polder map of Gly-DCA at the contour level 3.0 σ is shown as a raspberry mesh. **b**) Protein mapping of hSHMT1 using the Eisenberg hydrophobic scale.

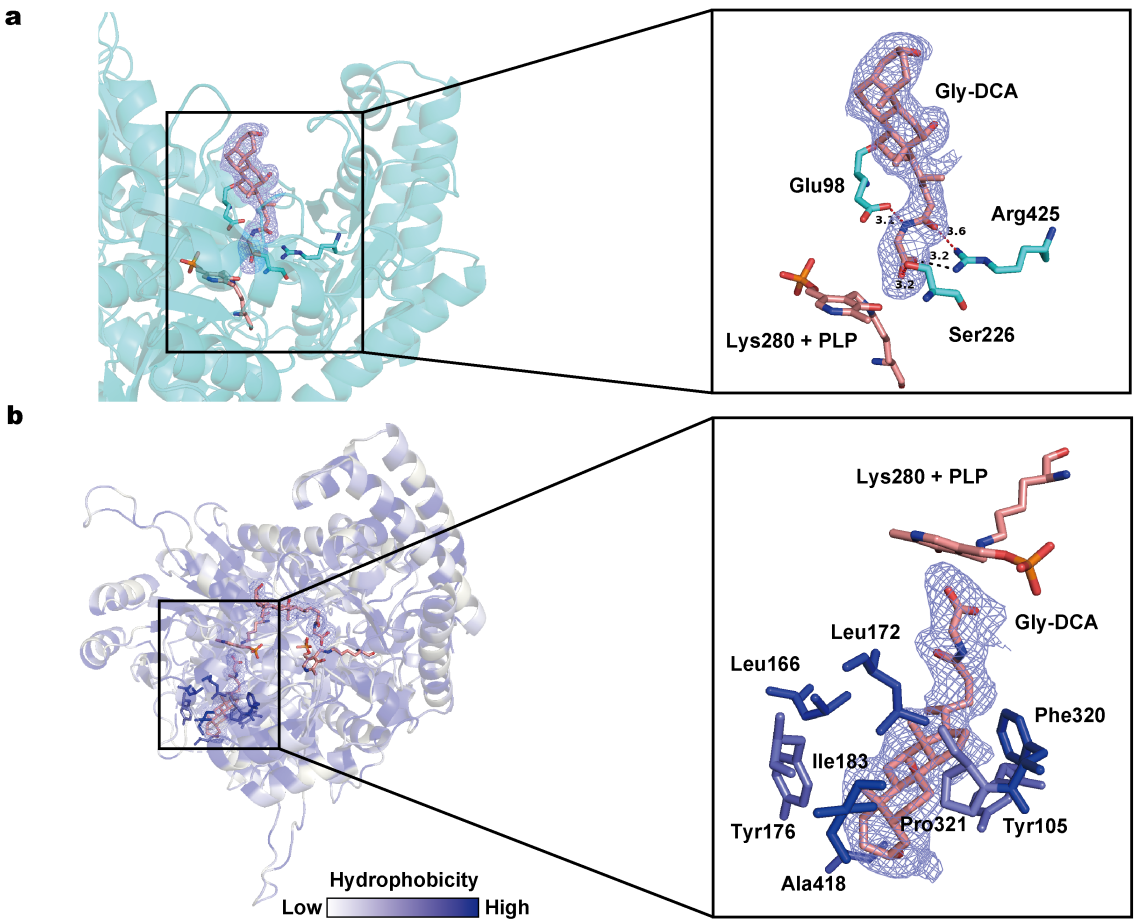

Figure S3. Crystal structure of hSHMT2–Gly-DCA complex, Related to Figure 3

a) Interaction between hSHMT2 and Gly-DCA. Gly-DCA is shown as a stick model with carbon displayed in salmon. Hydrogen bonding and salt bridge are represented as red dotted line and black dotted line, respectively. Polder map of Gly-DCA at the contour level 3.0 σ is displayed as purple mesh. **b**) Protein mapping of hSHMT2 using the Eisenberg hydrophobic scale.

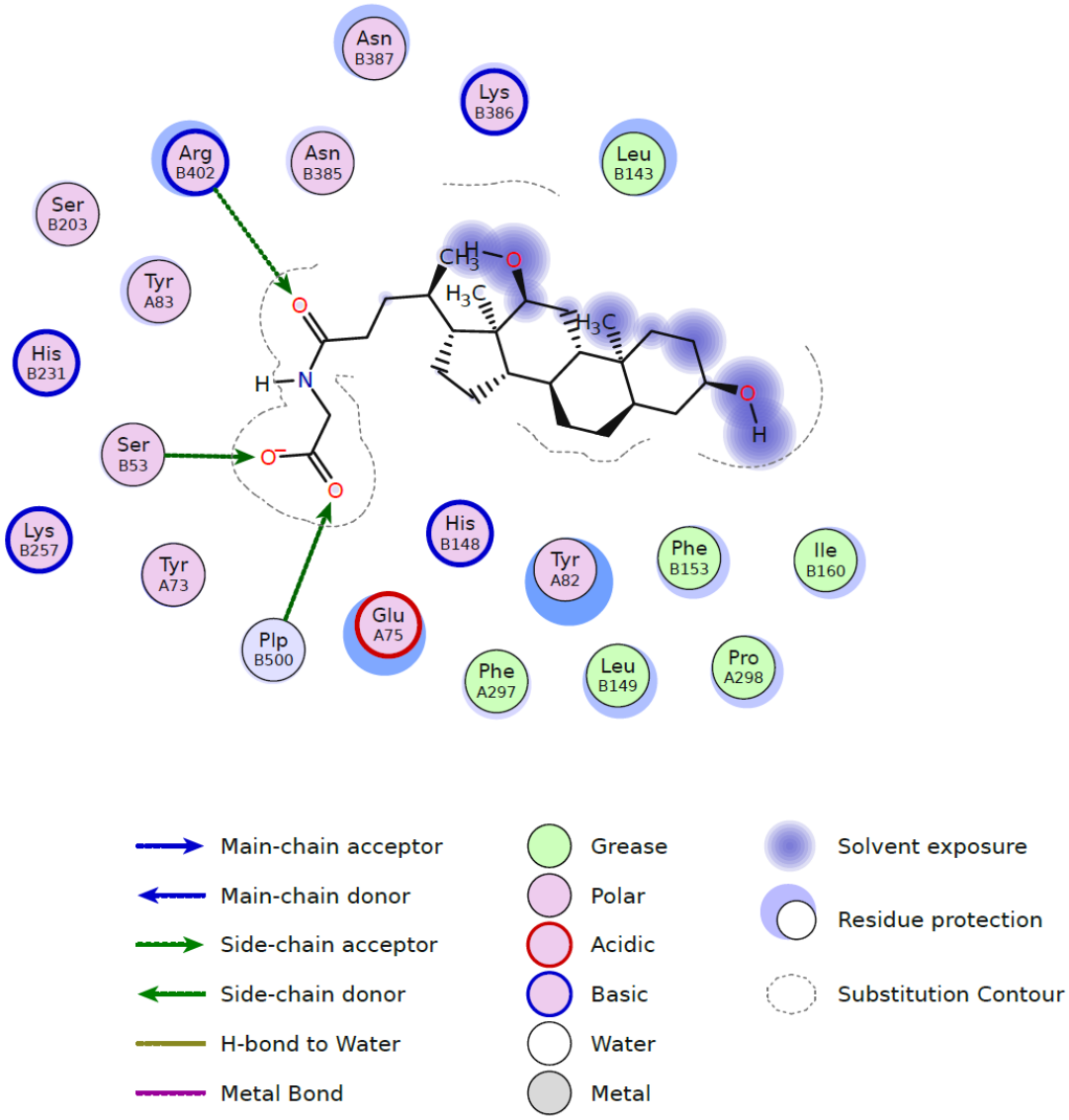

Figure S4. 2D interaction map of hSHMT1–Gly-DCA complex generated with FLEV (Clark and Labute, 2007), Related to Figure 2

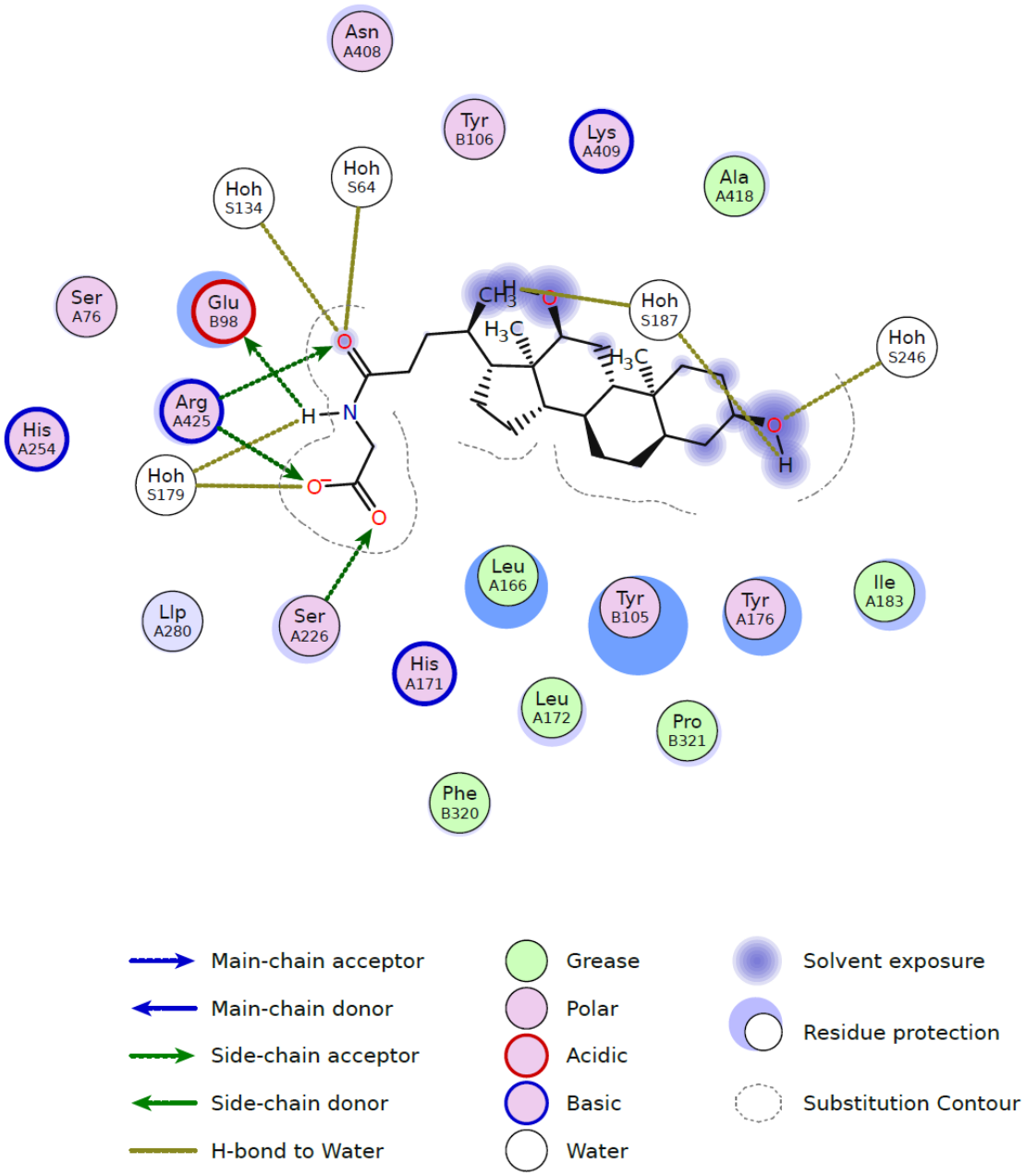

Figure S5. 2D interaction map of hSHMT2–Gly-DCA complex generated with FLEV, Related to Figure 3

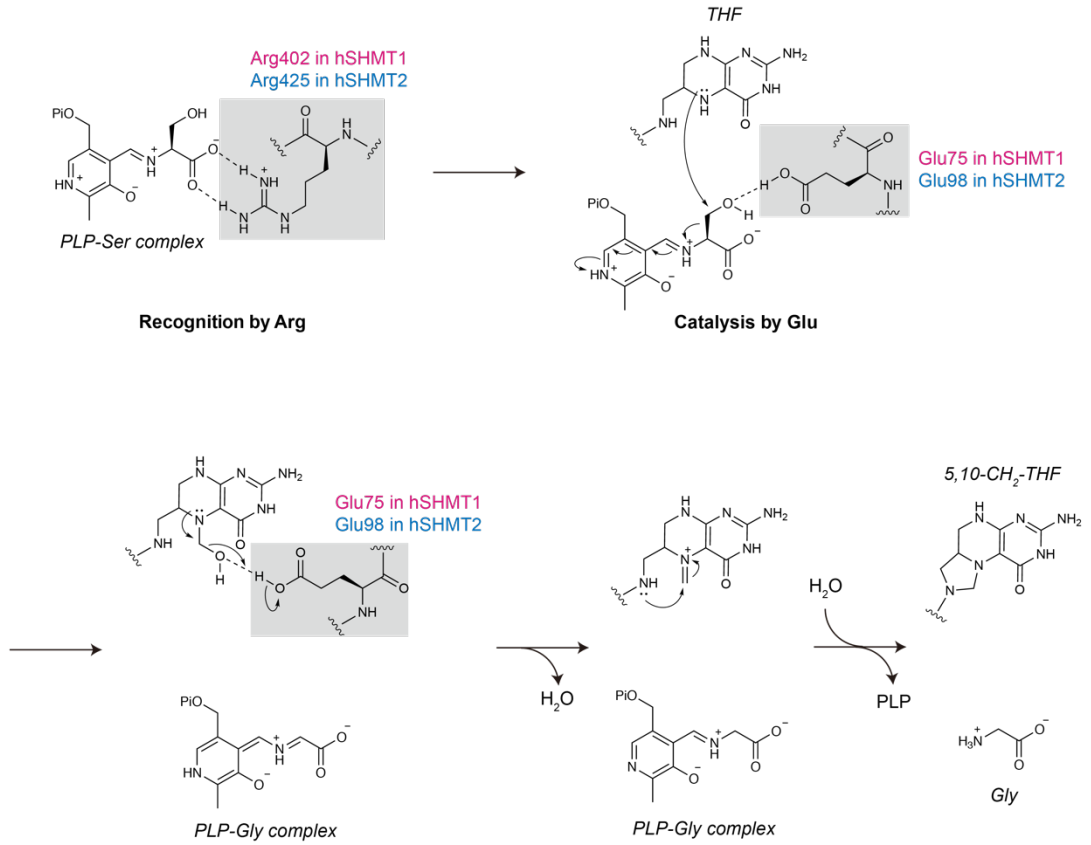

Figure S6. Proposed mechanism of SHMT-catalyzed Ser-Gly Conversion, Related to Figure 2 and 3

Two catalytic mechanisms have been proposed (Szebenyi et al., 2004; Schirch and Szebenyi, 2005; Appaji et al., 2003). Catalytic mechanism in conjunction with folate is shown in this Figure. Pi = $–PO_3^{2–}$, THF = tetrahydrofolate, PLP = pyridoxal 5′-phosphate, CH_2-THF = *N*-5,*N*-10-methylenetetrahydrofolate.

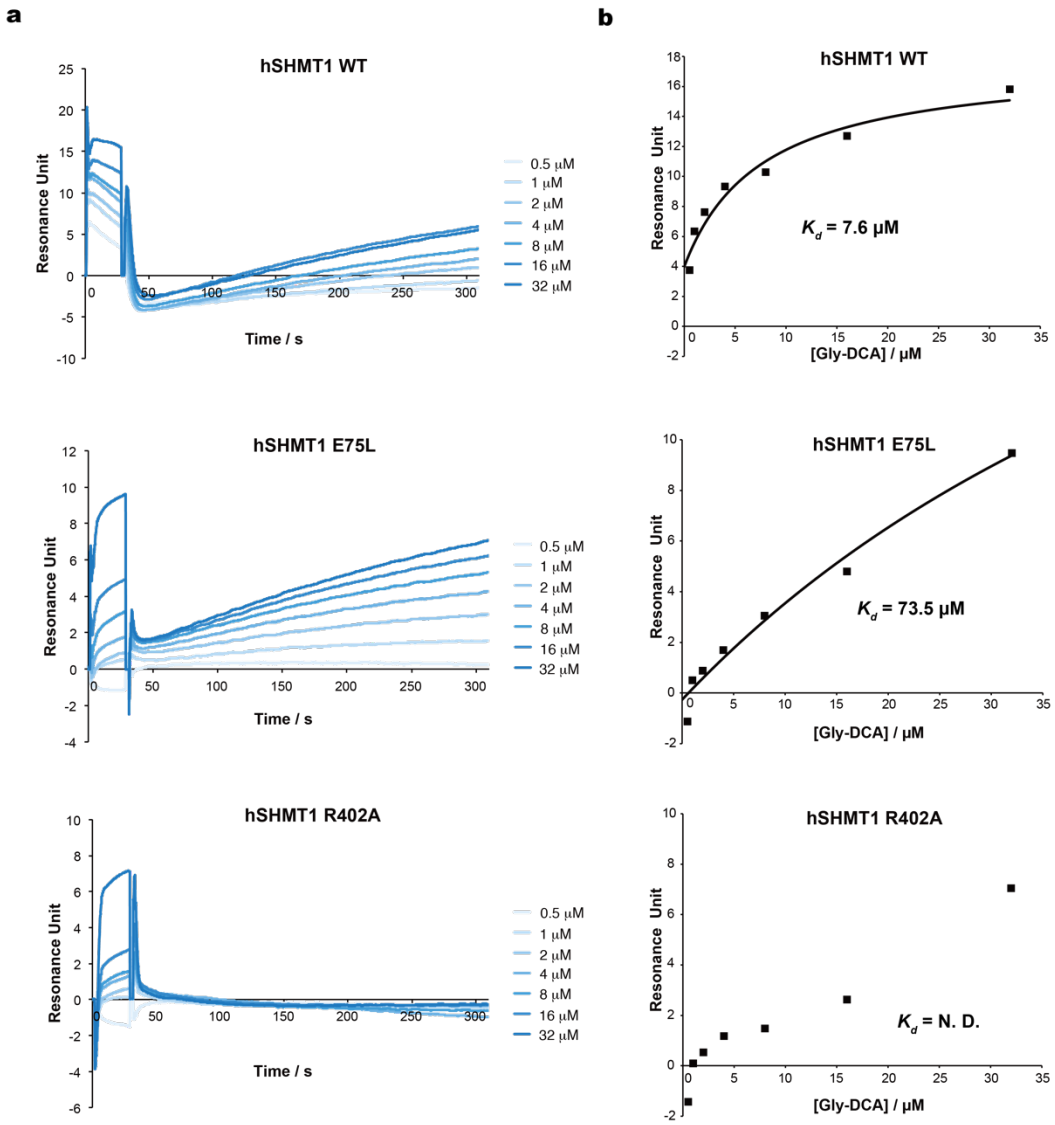

Figure S7. Mutation study based on binding affinity analysis for WT or mutant hSHMT1, Related to Figure 2 and 3

All the experiments were performed using Biacore 8K instrument. His_6-hSHMT1 WT or mutant was captured on Sensor chip NTA in each cycle. As an analyte, Gly-DCA was diluted with running buffer (10 mM HEPES pH 7.5, 100 mM NaCl, 2 mM β-mercaptoethanol, 0.01% (v/v) Tween20, 5% (v/v) DMSO) to a final concentration of 32, 16, 8, 4, 2, 1, and 0.5 μM. Contact time was 30 seconds, and dissociation time was 300

seconds. Binding data were analyzed in the Biacore 8K evaluation software. K_d value was calculated using the Scatchard method. **a**) Respective sensorgram. **b**) Binding affinity analysis.

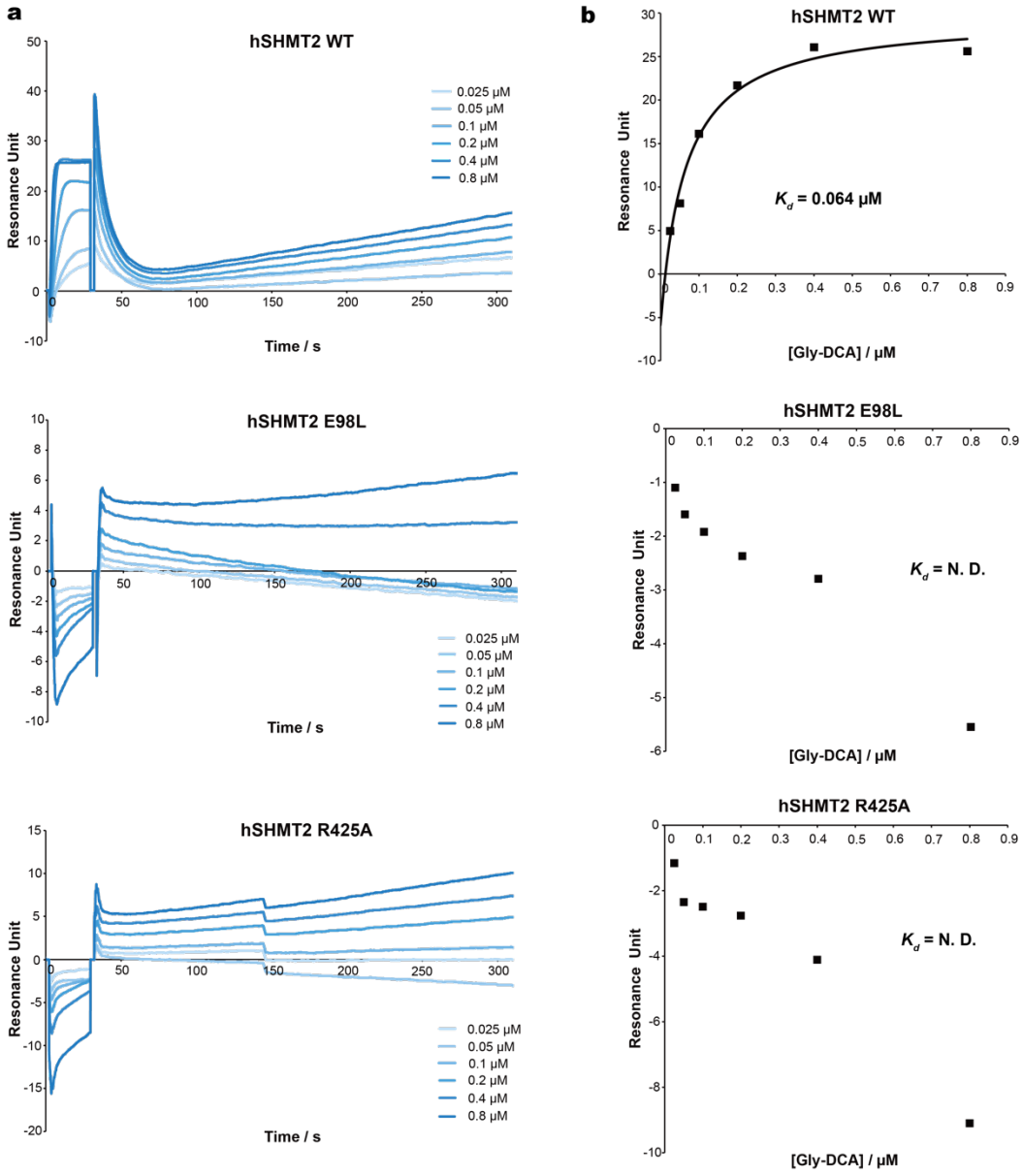

Figure S8. Mutation study based on binding affinity analysis for WT or mutant hSHMT2, Related to Figure 2 and 3

All the experiments were performed using Biacore 8K instrument. His_6-hSHMT2 WT or mutant was captured on Sensor chip NTA in each cycle. As an analyte, Gly-DCA was diluted with running buffer (10 mM HEPES pH 7.5, 200 mM NaCl, 2 mM *β*-mercaptoethanol, 50 μM PLP, 0.01% (v/v) Tween20, 5% (v/v) DMSO) to a final

concentration of 0.8, 0.4, 0.2, 0.1, 0.05, and 0.025 μM. Contact time was 30 seconds, and dissociation time was 300 seconds. Binding data were analyzed in the Biacore 8K evaluation software. K_d value was calculated using the Scatchard method. **a**) Respective sensorgram. **b**) Binding affinity analysis.

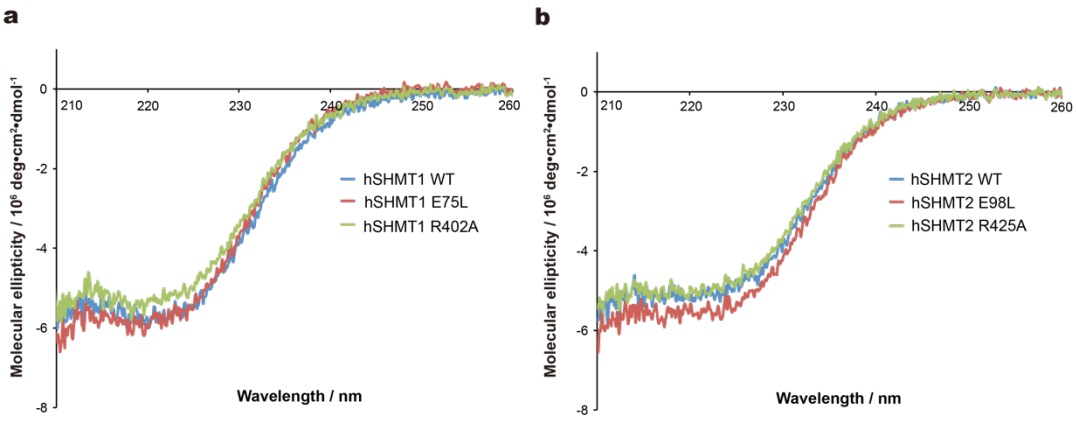

Figure S9. Circular dichroism spectra, Related to Figure 2 and 3

a) Circular dichroism spectra for WT or mutant hSHMT1. Conditions were as follows: 10 mM HEPES pH 7.5, 100 mM NaCl, 2 mM β-mercaptoethanol, 1.8 µM (0.1 mg/mL) hSHMT1 WT, E75L or R402A, 25 °C. **b)** Circular dichroism spectra for WT or mutant hSHMT2. Conditions were as follows: 10 mM HEPES pH 7.5, 200 mM NaCl, 2 mM β-mercaptoethanol, 50 µM PLP, 1.8 µM (0.1 mg/mL) hSHMT2 WT, E98L or R425A, 25 °C.

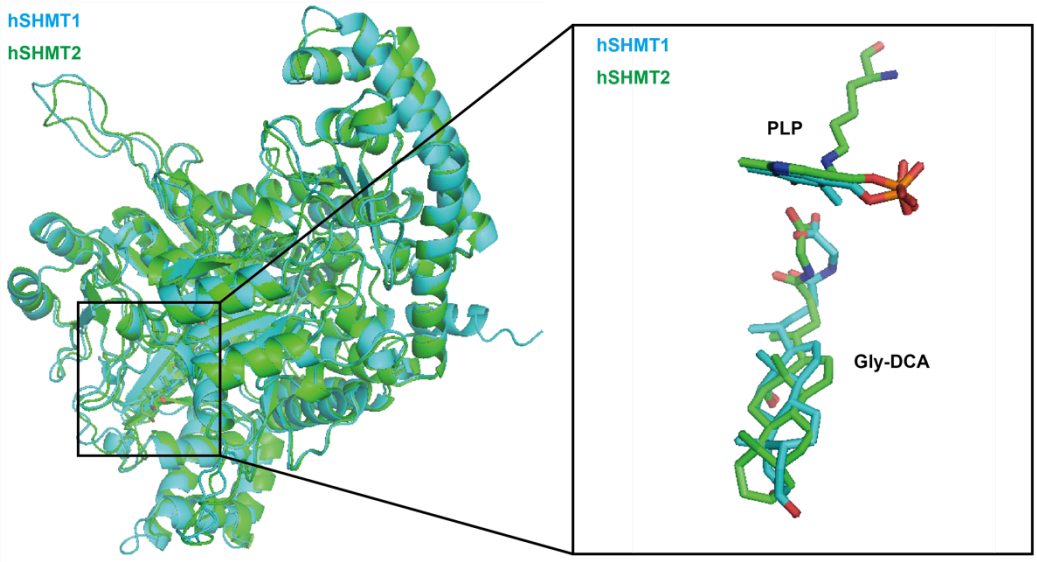

Figure S10. Superimposition of hSHMT1–Gly-DCA complex on hSHMT2–Gly-DCA complex, Related to Figure 4

hSHMT1 and hSHMT2 are represented as cartoon and Gly-DCA is shown as stick model.

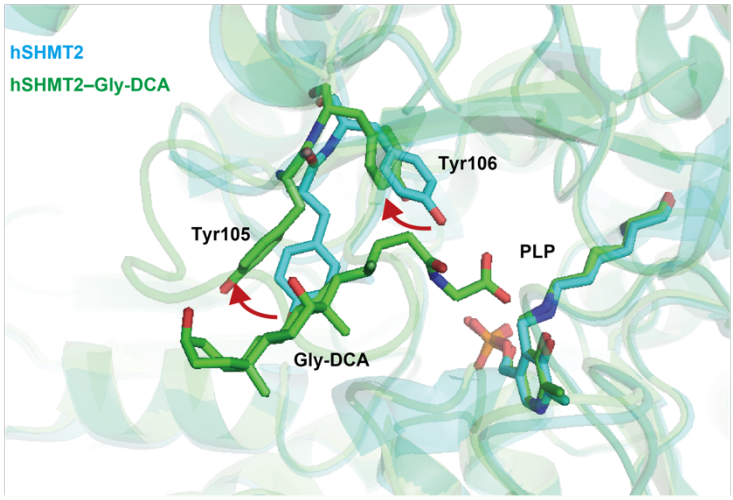

Figure S11. Superimposition of hSHMT2–Gly-DCA complex on apo hSHMT2 (PDB ID: 4PVF), Related to Figure 5

hSHMT2 is represented as cartoon, and Gly-DCA and partial amino acid residues are shown as stick model.

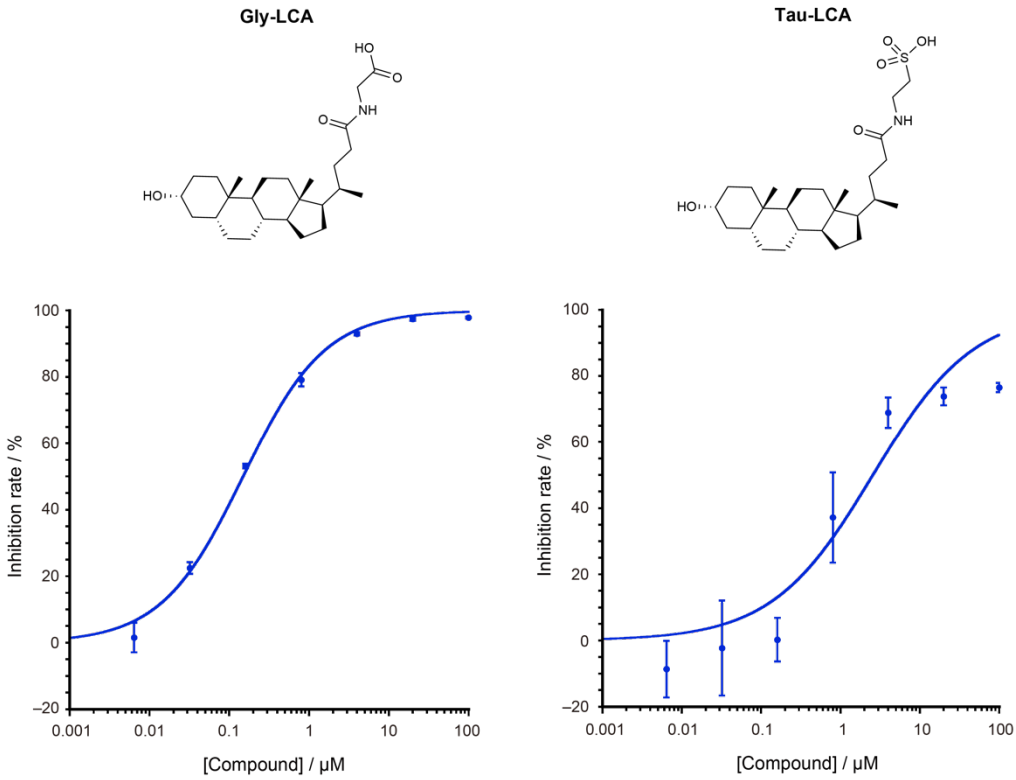

Figure S12. Inhibition properties of Gly-LCA and Tau-LCA against hSHMT2, Related to Figure 5

Inhibition rates against hSHMT2 activity were determined by HPLC analysis of Ser-Gly conversion in the presence of various concentrations of Gly-LCA and Tau-LCA. Assay conditions: 10 mM HEPES pH 7.5, 100 mM NaCl, 0.5 mM EDTA, 1 mM DTT, 1 mM L-Ser, 0.2 mM THF, 0.36 μM hSHMT2, 1% (v/v) DMSO, 25 °C, 30 min. Error bars represent s.d., n = 3.

2. Supplemental Tables

Table S1. Crystallographic data collection and refinement statistics, Related to Figure 2 and 3

Data collection	**hSHMT1 –Gly-DCA**		**hSHMT2 –Gly-DCA**
	Uncorrected	Anisotropy scaled	-
PDB ID	-	6M5W	6M5O
space group	*P* 6_2 2 2		*P* 6_5 2 2
unit cell dimensions			
a=b, c (Å)	152.75, 235.93		159.84, 211.21
wavelength (Å)	1.0000		1.0000
resolution (Å)*	46.03–3.10 (3.21–3.10)		49.37-2.30 (2.38–2.30)
R_{merge}	0.54 (4.96)	-	0.32 (1.88)
R_{meas}	0.55 (5.07)	-	0.32 (1.92)
R_{pim}	0.12 (1.06)	-	0.07 (0.40)
$I/\sigma(I)$	10.1 (1.1)	-	12.4 (2.3)
$CC_{1/2}$	1.0 (0.6)	-	1.0 (0.8)
Wilson B-factor (Å^2)	71.60	44.09	35.23
completeness (%)	99.9 (99.9)	-	100.0 (100.0)
Redundancy	21.9 (22.4)	-	22.3 (22.5)
Refinement statistics			
resolution (Å)	46.03–3.10	46.03–3.10	49.36–2.30
R_{work}	-	0.1822	0.201
R_{free}	-	0.2274	0.256
No. of protein atoms	-	3616	7,194
No. of heterogen atoms	-	89	196
No. of water molecules	-	0	490
unique reflections	-	30073	70,968
Average B-factor (Å^2)	-	34.99	42.00
R. M. S. deviations			
bonds (Å)	-	0.003	0.010
angles (°)	-	0.58	0.96
Ramachandran plot (%)			
Favored region	-	91.9	94.1
Allowed region	-	7.9	5.0
Outlier region	-	0.2	0.9

*Values in parentheses are for the highest-resolution shell.

Table S2. Completeness of the data for SHMT1–Gly-DCA, Related to Figure 2

After anisotropy correction	
Resolution range (Å)	Completeness (%)
3.70 - 3.51	59
3.51 - 3.35	31
3.35 - 3.22	16
3.22 - 3.10	5

No anisotropy correction	
Resolution range (Å)	Completeness (%)
3.70 - 3.51	100
3.51 - 3.35	100
3.35 - 3.22	100
3.22 - 3.10	100

3. Transparent Methods

Synthesis

Generals

Cholic acid (CA), deoxycholic acid (DCA), chenodeoxycholic acid (CDCA), ursodeoxycholic acid (UDCA), and lithocholic acid (LCA) were purchased as free acids (CA, DCA, LCA: Nacalai tesque, CDCA: Kanto chemical, UDCA: Tokyo Chemical Industry). Taurocholic acid (Tau-CA), taurodeoxycholic acid (Tau-DCA, **3**), taurochenodeoxycholic acid (Tau-CDCA), tauroursodeoxycholic acid (Tau-UDCA), and taurolithocholic acid (Tau-LCA) were purchased as sodium salts (Tau-CA: Tokyo Chemical Industry, Tau-DCA, Tau-CDCA, Tau-LCA: Cayman Chemical Company, Tau-UDCA: Nacalai tesque). Glycocholic acid (Gly-CA), glycodeoxycholic acid (Gly-DCA), glycochenodeoxycholic acid (Gly-CDCA), glycoursodeoxycholic acid (Gly-UDCA), and glycolithocholic acid (Gly-LCA) were synthesized as free acids through the standard condensation of an unconjugated bile acid and glycine methyl ester hydrochloride followed by deprotection of methyl ester group. Condensation was performed following previous reports (Incerti et al., 2013; Zhang et al., 2017; Simpson et al., 2010; Hirayama et al., 2003; Kolhatkar and Polli, 2012) with slight modifications. Deprotection was performed according to the previous reports (Incerti et al., 2013; Zhang et al., 2017) with slight modifications. Compound **2** was synthesized following previous reports (Simpson et al, 2010) with slight modifications.

Unless otherwise noted, all reagents and dry solvents were purchased from commercial suppliers and used without further purification. Nuclear magnetic resonance (NMR) spectra were measured and recorded using a JEOL ECS400 (^{1}H 400 MHz, ^{13}C 100 MHz) spectrometer or a Bruker Ascend 500 NMR (^{1}H 500 MHz, ^{13}C 125 MHz) spectrometer. Chloroform-d_1 (7.26 ppm) and methanol-d_4 (3.31 ppm) were used as internal standards for ^{1}H NMR. Chloroform-d_1 (77.0 ppm), methanol-d_4 (49.0 ppm), and dimethylsulfoxide-d_6 (39.5 ppm) were used as internal standards for ^{13}C NMR. Data are reported as follows: chemical shift, multiplicity (s = singlet, brs = broad singlet, t = triplet, q = quartet, m = multiplet), coupling constant (Hz), and integration. High-resolution mass spectra (HRMS) were measured using a Bruker micrOTOF II (ESI).

Synthesis of compound S1

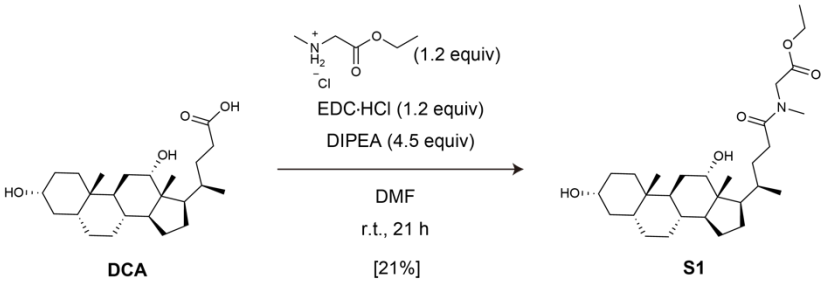

To a solution of DCA (151 mg, 385 μmol, 1.0 equiv), 1-(3-dimethylaminopropyl)-3-ethylcarbodiimide hydrochloride (EDC·HCl) (89.5 mg, 467 μmol, 1.2 equiv), and *N*,*N*-diisopropylethylamine (DIPEA) (300 μL, 1.72 mmol, 4.5 equiv) in *N*,*N*-dimethylformamide (DMF) (4.0 mL) in a 25 mL round-bottom flask was added sarcosine ethyl ester hydrochloride (71.4 mg, 465 μmol, 1.2 equiv). The reaction mixture was stirred for 21 h at ambient temperature. The mixture was extracted with ethyl acetate, and then the separated organic layer was washed with saturated aqueous NH_4Cl (×3). After drying over anhydrous Na_2SO_4, the solvent was removed under reduced pressure. The residue was purified by flash column chromatography on silica gel with dichloromethane-methanol (from 100%-0% to 80%-20%) to give compound **S1** as white foam (39.5 mg, 21 %). ^{1}H NMR ($CDCl_3$, 400 MHz) δ = 0.65/0.66 (s, 3 H, cis/trans), 0.88 (s, 3 H), 0.90–2.45 (m, 34 H), 2.94/3.06 (s, 3 H, cis/trans), 3.53–3.61 (m, 1 H), 3.95 (brs, 1 H), 4.02/4.08 (s, 2 H, cis/trans), 4.15/4.21 (q, *J* = 7.2 Hz, 2 H, cis/trans); ^{13}C NMR (DMSO-d_6, 100 MHz) δ = 12.4, 14.1, 17.1, 17.1, 23.1, 23.5, 26.1, 27.0, 27.1, 27.2, 28.6, 29.0, 29.4, 30.2, 30.7, 30.9, 32.9, 33.8, 34.2, 35.0, 35.1, 35.1, 35.6, 36.2, 36.3, 41.6, 46.0, 46.0, 46.3, 47.5, 49.0, 50.9, 60.3, 60.8, 69.9, 71.0, 79.2, 169.4, 169.7, 173.1, 173.2 (cis/trans isomerization gave more signals than expected.); HRMS (ESI): *m/z* calc. for $C_{29}H_{49}NNaO_5^+$ $[M+Na]^+$ = 514.3503, found = 514.3514.

Synthesis of compound 1

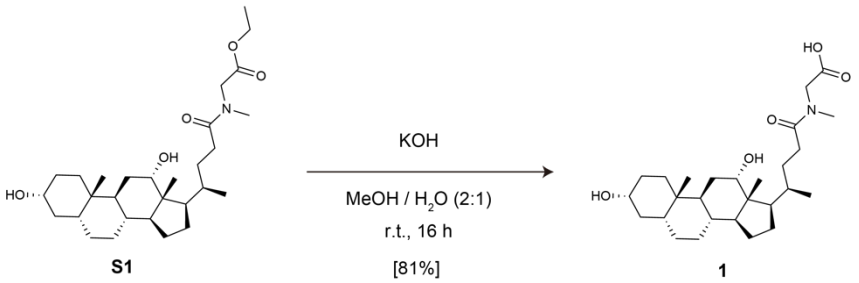

To a solution of compound **S1** (10.1 mg, 20.7 μmol) in methanol (1.0 mL) was added a solution of 5 M KOH in water (0.5 mL), and the mixture was stirred at room temperature for 16 h. Solvent was removed under reduced pressure. The solution was acidified with 9.4 M hydrochloric acid until a precipitate was formed. After the resulting suspension was filtered, the white residue was washed with water to give the compound **1** as a white solid (7.7 mg, 81%). ^{1}H NMR (methanol-d_4, 400 MHz) δ = 0.71/0.72 (s, 3 H, cis/trans), 0.94 (s, 3 H), 0.98–2.53 (m, 29 H), 2.94/3.12 (s, 3 H, cis/trans), 3.53 (m, 1 H), 3.95–3.97 (m, 1 H), 4.09/4.17 (s, 2 H, cis/trans); ^{13}C NMR (DMSO-d_6, 100 MHz) δ = 12.4, 17.1, 17.1, 23.1, 23.5, 26.1, 27.0, 27.1, 27.2, 28.6, 29.0, 29.4, 30.2, 30.7, 30.9, 32.9, 33.8, 35.0, 35.1, 35.1, 35.6, 36.1, 36.3, 41.6, 46.0, 46.3, 47.5, 48.9, 69.9, 71.0, 170.9, 173.0 (cis/trans isomerization gave more signals than expected.); HRMS (ESI): *m/z* calc. for $C_{27}H_{45}NNaO_5^+$ $[M+Na]^+$ = 486.3190, found = 486.3212.

Synthesis of compound S2

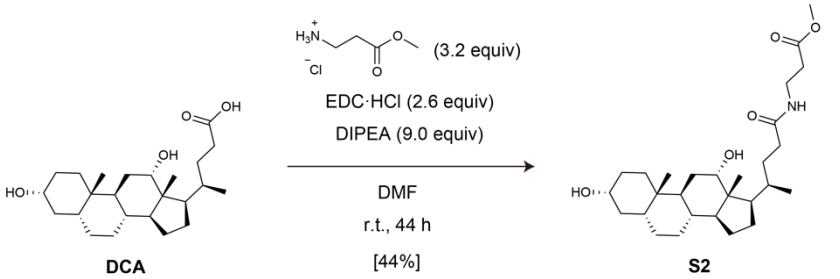

To a solution of DCA (99.2 mg, 253 μmol, 1.0 equiv), EDC·HCl (65.3 mg, 341 μmol, 1.3 equiv), and DIPEA (200 μL, 1.15 mmol, 4.5 equiv) in DMF (2.0 mL) in a 25 mL round-bottom flask was added *β*-alanine methyl ester hydrochloride (47.6 mg, 341 μmol, 1.3

equiv). After the resulting mixture was stirred for 27 h at ambient temperature, EDC·HCl (60.6 mg, 316 μmol, 1.2 equiv), DIPEA (200 μL, 1.15 mmol, 4.5 equiv) and β-alanine methyl ester hydrochloride (63.9 mg, 458 μmol, 1.8 equiv) were further added to the solution. After the resulting mixture was stirred for 17 h at ambient temperature, saturated $NaHCO_3$ aq. was added, and then the mixture was extracted with ethyl acetate. After drying over anhydrous Na_2SO_4, the solvent was removed under reduced pressure, and the residue was purified by flash column chromatography on silica gel with dichloromethane-methanol (from 100%-0% to 80%-20%) to give compound **S2** as white foam (52.9 mg, 44%). ^{1}H NMR ($CDCl_3$, 400 MHz) δ = 0.63 (s, 3 H), 0.87 (s, 3 H), 0.92–2.23 (m, 29 H), 2.49–2.52 (m, 4 H), 3.46 (q, *J* = 6.0 Hz, 2 H), 3.52–3.60 (m, 1 H), 3.66 (s, 3 H), 3.93 (brs, 1 H), 6.34 (t, *J* = 6.0 Hz, 1 H); ^{13}C NMR ($CDCl_3$, 100 MHz) δ = 12.6, 17.3, 23.1, 23.6, 26.1, 27.1, 27.5, 28.5, 30.3, 31.5, 33.3, 33.5, 33.8, 34.1, 34.7, 35.2, 35.9, 36.3, 42.0, 46.4, 46.9, 48.0, 51.7, 71.6, 73.0, 173.1, 173.7 (1C was not determined because of peak overlapping.); HRMS (ESI): *m/z* calc. for $C_{28}H_{47}NNaO_5^+$ $[M+Na]^+$ = 500.3346, found = 500.3366.

Synthesis of compound 4

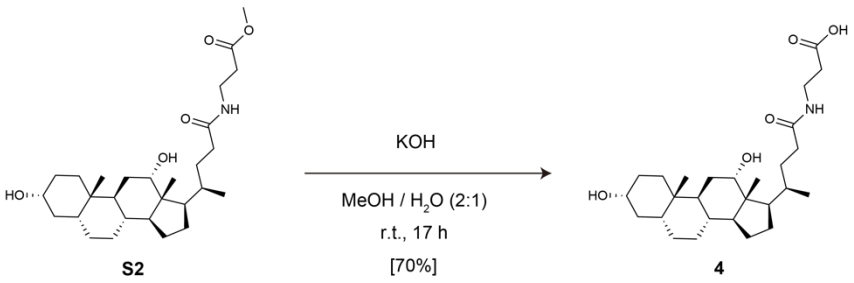

To a solution of compound **S2** (24.0 mg, 50.2 μmol) in methanol (2.0 mL) was added a solution of 5 M KOH in water (1.0 mL) and the mixture was stirred at room temperature for 17 h. Solvent was removed under reduced pressure and the solution was acidified with concentrated hydrochloric acid until a precipitate was formed. The resulting suspension was filtered and the white residue was washed with water to give the compound **4** as a white solid (16.3 mg, 70%). ^{1}H NMR (methanol-*d*$_4$, 400 MHz) δ = 0.71 (s, 3 H), 0.93 (s, 3 H), 0.98–1.93 (m, 27 H), 2.06–2.28 (m, 2 H), 2.50 (t, *J* = 6.8 Hz, 2 H), 3.41 (t, *J* = 6.8 Hz, 2 H), 3.49–3.56 (m, 1 H), 3.95 (brs, 1 H); ^{13}C NMR (methanol-*d*$_4$, 100 MHz) δ = 13.2,

17.6, 23.7, 24.9, 27.5, 28.4, 28.7, 29.9, 31.1, 33.3, 34.0, 34.7, 34.8, 35.3, 36.4, 36.4, 36.8, 37.2, 37.5, 43.6, 47.6, 48.1, 49.3, 72.5, 74.1, 173.8, 177.0; HRMS (ESI): *m/z* calc. for $C_{27}H_{45}NNaO_5$ $[M+Na]^+$ = 486.3190, found = 486.3213.

hSHMT1 expression, purification, and crystallization

The pET28a(+)-hSHMT1 plasmid was constructed as described previously (Nonaka et al., 2019). The pET28a(+)-hSHMT1 plasmid was transformed into E. coli BL21(DE3)pLysS cells. The transformed E. coli cells were added to LB medium containing 20 μg mL^{-1} kanamycin and 20 μg mL^{-1} chloramphenicol, incubated at 37 °C overnight, and then diluted with LB medium (1 L). The culture was then incubated until the OD_{600} reached 0.6. IPTG (final concentration of 0.5 mM) was added to the culture to induce expression. The culture was maintained at 37 °C for 4 h, and then harvested by centrifugation at 3,000 × g for 10 min at 4 °C. Cells were suspended in lysis buffer (20 mM Tris-HCl pH 8.0, 20 mM imidazole, 300 mM NaCl, 100 μM PMSF) and then disrupted by ultrasonication. Cellular debris was removed by centrifugation at 10,000 × g for 30 min at 4 °C. Purification was conducted using Ni-NTA resin. The collected fractions were dialyzed using a 100-kDa cutoff filter (first: 10 mM HEPES pH 7.4, 300 mM NaCl, 2 mM β-mercaptoethanol and 0.5 mM EDTA at 4 °C for 1 h; second: 10 mM HEPES pH 7.4, 200 mM NaCl, 2 mM β-mercaptoethanol and 0.5 mM EDTA at 4 °C overnight). The obtained proteins were analyzed by SDS-PAGE. hSHMT1 activity was determined following a standard protocol and using DL-erythro-β-phenylserine as substrate (Webb and Matthews, 1995). The amount of enzyme producing 1 μmol of benzaldehyde over a period of 1 h at 25 °C was defined as 1 unit. Reaction conditions: 50 mM HEPES pH 7.5, 100 mM NaCl, 0.5 mM EDTA, 1 mM DTT, and 10 mM DL-erythro-β-phenylserine.

For crystallization and differential scanning calorimetry (DSC), samples were loaded into a HiLoad™ 26/600 Superdex™ 200 pg (GE Healthcare) and eluted using SEC buffer (10 mM HEPES pH 7.4, 100 mM NaCl, 0.5 mM EDTA, and 2 mM β-mercaptoethanol). Objective fraction was concentrated using Amicon Ultra 30K. hSHMT1 was crystallized via sitting vapor-diffusion method by mixing 0.5 μL protein (11 mg mL^{-1}) with 0.5 μL reservoir solution at 20 °C. The hexagonal bipyramidal crystals grew in a reservoir solution containing 0.2 M potassium chloride, 0.05 M HEPES pH 7.5, and 35% (v/v)

pentaerythritol propoxylate (5/4 PO/OH). The crystal was briefly soaked in a cryoprotectant solution composed of 500 μM Gly-DCA and 5% (v/v) DMSO dissolved in their corresponding mother liquors, and then flash-cooled directly in a liquid-nitrogen stream at 77 K.

hSHMT2 expression, purification, and crystallization

The pET28a(+)-hSHMT2 plasmid was constructed as described previously (Nonaka et al., 2019). The pET28a(+)-hSHMT2 plasmid was transformed into E. coli BL21(DE3)pLysS cells. Transformed E. coli cells were added to LB medium containing 20 μg mL^{-1} kanamycin and 20 μg mL^{-1} chloramphenicol, incubated at 37 °C overnight, and then diluted with LB medium (1 L). The culture was incubated until the OD_{600} reached 0.6. After cooling the medium to 16 °C, IPTG (final concentration of 0.5 mM) was added to induce expression. The culture was maintained at 16 °C for 16 h before harvesting by centrifugation at 3,000 × g for 10 min at 4 °C. Cells were suspended in lysis buffer (50 mM HEPES pH 7.5, 200 mM NaCl, 10% glycerol, 10 μM PLP, and 100 μM PMSF) and then disrupted by ultrasonication. Cellular debris was removed by centrifugation at 10,000 × g for 30 min at 4 °C. Purification was conducted using Ni-NTA resin. The collected fractions were dialyzed using a 50-kDa cutoff filter (first: 10 mM HEPES pH 7.4, 300 mM NaCl, 2 mM β-mercaptoethanol, 0.5 mM EDTA, and 50 μM PLP at 4 °C for 1 h; second: 10 mM HEPES pH 7.4, 200 mM NaCl, 2 mM β-mercaptoethanol, 0.5 mM EDTA, and 50 μM PLP at 4 °C overnight). The obtained proteins were analyzed by SDS-PAGE. hSHMT2 activity was determined following a standard protocol and using DL-erythro-β-phenylserine as substrate (Webb and Matthews , 1995). The amount of enzyme producing 1 μmol of benzaldehyde over a period of 1 h at 25 °C was defined as 1 unit. Reaction conditions: 50 mM HEPES pH 7.5, 100 mM NaCl, 0.5 mM EDTA, 1 mM DTT, and 10 mM DL-erythro-β-phenylserine.

For crystallization, DSC and isothermal titration calorimetry (ITC), samples were loaded into a HiLoad™ 26/600 Superdex™ 200 pg (GE Healthcare) and eluted using SEC buffer (10 mM HEPES pH 7.4, 200 mM NaCl, 0.5 mM EDTA, 2 mM β-mercaptoethanol, and 50 μM PLP). Objective fraction was concentrated using Amicon Ultra 30K. hSHMT2 was crystallized via sitting vapor-diffusion method by mixing 0.5 μL protein (9 mg mL^{-1}) containing 200 μM Gly-DCA and 2% (v/v) DMSO with 0.5 μL

reservoir solution at 20 °C. The needle-shaped crystals grew in a reservoir solution containing 0.1 M Tris hydrochloride pH 8.5 and 8% (w/v) polyethylene glycol 8,000. Each crystal was briefly soaked in a cryoprotectant solution consisting of 200 μM Gly-DCA, 2% (v/v) DMSO, and 22% (v/v) glycerol dissolved in their corresponding mother liquors, and then flash-cooled directly using a liquid-nitrogen stream at 77 K.

Data collection and structure determination

X-ray diffraction datasets were collected on a RIKEN Structural Genomics Beamline II (BL26B2) at SPring-8 (Ueno et al., 2006) using a 120-μm-wide, 120-μm-high beam. The diffraction data were processed using XDS programs (Kabsch et al., 2010), and structure was solved by molecular replacement, using the structure of hSHMT1 (PDB ID: 1BJ4) or hSHMT2 (PDB ID: 4PVF) as a search model with phenix.phaser (Adams et al., 2010). The resultant structure was iteratively refined using phenix.refine, and manually rebuilt in Coot (Emsley et al., 2010). In the Ramachandran plot, 91.9% of residues were in favored regions and 7.9% of residues were in allowed regions for the hSHMT1–Gly-DCA complex; for the hSHMT2–Gly-DCA complex, 94.1% of residues were in favored regions, and 5.0% of residues were in allowed regions. Final refinement statistics are summarized in Table S1. As for the hSHMT1 structure, the data were truncated by the UCLA-MBI diffraction anisotropy server (Strong et al., 2006). The anisotropic resolution cut-off values along the a*, b*, and c* axes are 3.6 $Å^{-1}$, 3.7 $Å^{-1}$, and 3.1 $Å^{-1}$ respectively (Figure S1). The comparison of data completeness in truncated region at each resolution bin is summarized in Table S2. All figures were prepared using PyMOL (Schrödinger) or UCSF Chimera (Pettersen et al., 2004).

Inhibition assay of Ser-Gly conversion

The procedure was performed as described in our previous study (Nonaka et al., 2019) with a slight modification (THF = 0.2 mM).

Preparation of mutant hSHMT1

The plasmid for mutant hSHMT1 or hSHMT2 was prepared using an hSHMT1 or hSHMT2 plasmid with the following primers, respectively. Bold characters represent the site of introduced mutation.

hSHMT1 E75L Fw 5′-TCTCTTGGGTACCCGGGCCAGA-3′
hSHMT1 E75L Rv 5′-GGCCCGGGTACCCAAGAGAGTATTTGT-3′
hSHMT1 R402A Fw 5′-ACTGGCACTGGGGACCCCA-3′
hSHMT1 R402A Rv 5′-AGTGCCAGTCCACTGGGCC-3′
hSHMT2 E98L Fw 5′-TACTCGCTGGGTTATCCTGGCAAGAGA-3′
hSHMT2 E98L Rv 5′-ATAACCCAGCGAGTACTTGTTGTTCAG-3′
hSHMT2 R425A Fw 5′-GCCTGGCACTTGGGGCCCC-3′
hSHMT2 R425A Rv 5′-CCAAGTGCCAGGCCGCCCG-3′
Mutant hSHMT1 or hSHMT2 was expressed, purified, and dialyzed in the same manner as hSHMT1 or hSHMT2, respectively.

Surface plasmon resonance (SPR)

All the experiments were performed using a Biacore 8K instrument (GE Healthcare). His_6-hSHMT was captured on Sensor chip NTA in each cycle. For hSHMT1 WT and mutant, as an analyte, Gly-DCA was diluted in running buffer [10 mM HEPES pH 7.5, 100 mM NaCl, 2 mM β-mercaptoethanol, 0.01% (v/v) Tween 20, and 5% (v/v) DMSO] to a final concentration of 32, 16, 8, 4, 2, 1, and 0.5 μM. For hSHMT2 WT and mutant, as an analyte, Gly-DCA was diluted in running buffer [10 mM HEPES pH 7.5, 200 mM NaCl, 2 mM β-mercaptoethanol, 50 μM PLP, 0.01% (v/v) Tween 20, and 5% (v/v) DMSO] to a final concentration of 0.8, 0.4, 0.2, 0.1, 0.05, and 0.025 μM. Contact time was 30 seconds, and dissociation time was 300 seconds. Binding data were analyzed using Biacore 8K evaluation software. K_d value was calculated using the Scatchard method.

Circular dichroism (CD)

All assays were performed using a Jasco spectropolarimeter with a 0.1-cm path length quartz cuvette at 25 °C in 10 mM HEPES pH 7.5, NaCl (100 mM for hSHMT1, 200 mM for hSHMT2), 2 mM β-mercaptoethanol, 50 μM PLP (only for hSHMT2), and 1.8 μM (0.1 mg/mL) hSHMT1 WT, mutant hSHMT1, hSHMT2 WT or mutant hSHMT2.

Isothermal titration calorimetry (ITC)

All experiments were performed in an iTC200 (Microcal). All assays were carried out at

37 °C and stirring rate of 750 rpm in 10 mM HEPES pH 7.5, 200 mM NaCl, 0.5 mM EDTA, 2 mM β-mercaptoethanol, 50 μM PLP and 3% (v/v) DMSO. hSHMT2 was placed into the cell at the concentration of 28.9 μM, and Gly-DCA was placed into the syringe at the concentration of 300 μM. The titration consisted of one-injection of 0.5 μL, followed by 12 injections of 3 μL, with an interval of 180 seconds. Thermodynamic parameters were calculated using Origin7 software. Experimental conditions (concentrations of salt and PLP) were slightly different for hSHMT1 (100 mM NaCl and 0 μM PLP) (Nonaka et al., 2019) and hSHMT2 (200 mM NaCl and 50 μM PLP), because hSHMT2 tends to aggregate and release PLP under the condition used for hSHMT1.

Differential scanning calorimetry (DSC)

All assays were carried out using a MicroCal PEAQ-DSC instrument (Malvern Panalytical) in the range of 20 to 110 °C, and at the speed of 1 °C/min, in 10 mM HEPES pH 7.5, NaCl (100 mM for hSHMT1, 200 mM for hSHMT2), 0.5 mM EDTA, 2 mM β-mercaptoethanol, 50 μM PLP (only for hSHMT2), 18 μM (1.0 mg/mL) hSHMT1 or hSHMT2, 50 μM Gly-DCA, and 1% (v/v) DMSO. Data were analyzed using a non-two-state denaturation model. Experimental conditions (concentrations of salt and PLP) were slightly different for hSHMT1 (100 mM NaCl and 0 μM PLP) and hSHMT2 (200 mM NaCl and 50 μM PLP), because hSHMT2 tends to aggregate and release PLP under the condition used for hSHMT1.

4. Supplemental References

Adams, P.D., Afonine, P.V., Bunkóczi, G., Chen, V.B., Davis, I.W., Echols, N., Headd, J.J., Hung, L.-W., Kapral., G., Grosse-Kunstleve, R.W. et al. (2010). PHENIX: a comprehensive Python-based system for macromolecular structure solution. Acta Crystallogr. D *66*, 213–221.

Appaji Rao, N., Ambili, M., Jala, V.R., Subramanya, H.S., and Savithri, H.S. (2003). Structure–function relationship in serine hydroxymethyltransferase. Biochim. Biophys. Acta *1647*, 24–29.

Clark, A.M., and Labute, P. (2007). 2D depiction of protein-ligand complexes. J. Chem. Inf. Model. *47*, 1933–1944.

Emsley, P., Lohkamp, B., Scott, W.G., and Cowtan, K. (2010). Features and development of Coot. Acta Crystallogr. D *66*, 486–501.

Hirayama, Y., Iwamura, M., and Furuta, T. (2003). Design, synthesis and photochemical properties of caged bile acids. *Bioorg.* Med. Chem. Lett. *13*, 905–908.

Incerti, M., Tognolini, M., Russo, S., Pala, D., Giorgio, C., Hassan-Mohamed, I., Noberini, R., Pasquale, E.B., Vicini, P., Piersanti, S., et al. (2013). Amino acid conjugates of lithocholic acid as antagonists of the EphA2 receptor. J. Med. Chem. *56*, 2936–2947.

Kabsch, W. (2010). XDS. Acta Crystallogr. *D 66*, 125–132.

Kolhatkar, V., and Polli, J.E. (2012). Structural requirements of bile acid transporters: C-3 and C-7 modifications of steroidal hydroxyl groups. Eur. J. Pharm. Sci. *46*, 86–99.

Nonaka, H., Nakanishi, Y., Kuno, S., Ota, T., Mochidome, K., Saito, Y., Sugihara, F., Takakusagi, Y., Aoki, I., Nagatoishi, S., et al. (2019). Design strategy for serine hydroxymethyltransferase probes based on retro-aldol-type reaction. Nat. Commun. *10*,

876.

Pettersen, E.F., Goddard, T.D., Huang, C.C., Couch, G.S., Greenblatt, D.M., Meng, E.C., and Ferrin, T. (2004). UCSF Chimera—A visualization system for exploratory research and analysis. J. Comput. Chem. *25*, 1605–1612.

Schirch, V., and Szebenyi, D.M.E. (2005). Serine hydroxymethyltransferase revisited. Curr. Opin. Chem. Biol. *9*, 482–487.

Simpson, M.G., Pittelkow, M., Watson, S.P., and Sanders, J.K.M. (2010). Dynamic combinatorial chemistry with hydrazones: cholate-based building blocks and libraries. Org. Biomol. Chem. *8*, 1173–1180.

Strong, M., Sawaya, M.R., Wang, S., Phillips, M. Cascio, D. and Eisenberg, D. (2006). Toward the structural genomics of complexes: crystal structure of a PE/PPE protein complex from Mycobacterium tuberculosis. Proc. Natl. Acad. Sci. U S A *103*, 8060–8065.

Szebenyi, D.M.E., Musayev, F.N., di Salvo, M.L., Safo, M.K., and Schirch, V. (2004). Serine hydroxymethyltransferase: Role of Glu75 and evidence that serine is cleaved by a retroaldol mechanism. Biochemistry *43*, 6865–6876.

Ueno, G., Kanda, H., Hirose, R., Ida, K., Kumasaka, T., and Yamamoto, M. (2006). RIKEN structural genomics beamlines at the SPring-8; high throughput protein crystallography with automated beamline operation. J. Struct. Funct. Genomics *7*, 15–22.

Webb, H.K., and Matthews, R.G. (1995). 4-Chlorothreonine is substrate, mechanistic probe, and mechanism-based inactivator of serine hydroxymethyltransferase. J. Biol. Chem. *270*, 17204–17209.

Zhang, L., Song, C., Miao, G., Zhao, L., Yan, Z., Li, J., and Wang, Y. (2017). Novel liver-targeted conjugates of glycogen phosphorylase inhibitor PSN-357 for the treatment of diabetes: Design, synthesis, pharmacokinetic and pharmacological evaluations. Sci. Rep. *7*, 42251.